Fluxional Molecules with Five Equivalent Atoms: Mid-infrared Spectroscopy of CH_5^+ and H_5^+

James N. Hodges

Research Prospectus for Preliminary Examination

February 11, 2013 10:30 AM

A133 Chemical and Life Sciences Laboratory

University of Illinois at Urbana-Champaign

I. INTRODUCTION

Infrared spectroscopy is arguably one of the most powerful tools that is available to chemistry and molecular physics. As such, rovibrational spectroscopy's applications in determining rotational transitions indirectly, and its use in the support of astronomical observations are described. A description of the accomplished work to date is provided. The remainder of the document describes proposed experiments targeted at understanding the spectra of highly fluxional molecules with five equivalent atoms.

A. Indirect Rotational Spectroscopy

Indirect rotational spectroscopy is a technique that calculates rotational transitions by measuring rovibrational transitions. This approach is useful in determining rotational transitions in the sub-millimeter/THz region. The nascent field of THz light generation and detection is an active area of research, but there are technical challenges to direct spectroscopy in this region. Infrared spectroscopy, on the other hand, is a mature field with well developed technology.

To determine a rotational transition via infrared spectroscopy, the difference between two rovibrational transitions must be determined. The calculation requires that these two transitions share a rotational level in either the lower vibrational state or the upper vibrational state. The difference does not represent a rotational transition but an energy level spacing.

In the case of a linear molecule, these differences correspond to two adjacent rotational energy levels, such as the $\Delta E_{J=2\leftarrow 0}$ energy level spacing. In the lower vibrational state, the pair of rovibrational transitions whose difference results in $\Delta E_{J=2\leftarrow 0}$ spacing are P(2) and R(0) as demonstrated in Figure 1. For the rotational energy level spacings in the upper vibrational level, the same energy level spacing can be determined by the difference in P(2) and R(2). After all the energy level spacings are known, knowledge of only a single rotational transition can be used to construct the entire rotational spectrum.

B. Astronomical Applications

Molecules with a small moment of inertia have a large rotational constant. For example, higher J rotational transitions exist in the terahertz regime for HCO^+ and N_2H^+. [1] The

lack of laboratory spectra limits the identification of astronomical species, which presents an obvious use for indirect rotational spectroscopy. Astronomical observations of an unknown molecular line are not unprecedented. The $J = 1 \leftarrow 0$ transition of HCO^+ was first discovered by astronomers, [2] and five years passed before the species was correctly identified by spectroscopists. [3] Now it is one of the most commonly observed astronomical molecules, and it may be found in a variety of astronomical environments. [4–7]

Indirect THz spectroscopy is especially noteworthy considering recent astronomical developments. Newly constructed telescopes such as the Atacama Large Millimeter and sub-millimeter Array (ALMA) and the Stratospheric Observatory For Infrared Astronomy (SOFIA) both have coverage in the THz region of the spectrum, which will allow for the observation of a wealth of lines that have not yet been identified.

By targeting molecules of astronomical interest, the rotational energy level spacings can be provided by measuring a fundamental vibrational band. Then possessing the required rotational transitions, the entire rotational spectrum can be calculated limited solely by the number the rovibrational lines and the precision and accuracy of the instrument. The calculated spectrum can be used to identify new species in the interstellar medium, assign lines that where previously unknown, and probe the environment in which the species was observed.

II. COMPLETED WORK

A. High Precision Mid-IR Spectroscopy

1. Instrument Description

Two years were spent developing and testing a new instrument designed to perform high precision, high sensitivity, mid-IR spectroscopy. The instrument is described by Crabtree *et al.*, which is attached for convenience. [8] The instrument employs a spectroscopic technique called Noise Immune Cavity Enhanced Optical Heterodyne Velocity Modulation Spectroscopy or NICE-OHVMS. This technique was developed in the near-IR by Siller *et al.* [9] and is a combination of velocity modulation spectroscopy (VMS) [10–12] and Noise Immune Cavity Enhanced Optical Heterodyne Molecular Spectroscopy (NICE-OHMS) [13, 14]

This instrument is the first application of NICE-OHVMS in the mid-IR, and it may be

seen in the block diagram in Figure 2. It uses a cw-optical parametric oscillator (cw-OPO) as the light source, which is tunable from 3.2 to 3.9 μm. The light is generated in a ytterbium doped fiber laser operating at 1064 nm, which is coupled into a fiber electro-optic modulator (EOM). The EOM is driven at $\sim$ 4 MHz to generate side bands for Pound-Drever-Hall (PDH) locking and is simultaneously driven at $\sim$ 80 MHz to generate heterodyne sidebands for spectroscopy. After amplification, the light then enters into a fiber amplifier intensifying the laser power to 10 W. After amplification, the light travels into a bow-tie cavity, which is resonant between 1.5 to 1.6 μm. The cavity is where the OPO process occurs. It is singly resonant so the sidebands are imprinted on the idler but not on the signal beam.

The idler beam is coupled into an external cavity for spectroscopy, which is PDH locked to the idler frequency. Corrections occurring below $\sim$ 100 Hz are made by adjusting the cavity length via a piezo-electric transducer (PZT) attached to a cavity mirror. Faster corrections are made by varying the length of the signal cavity of the OPO. Within the cavity is a liquid nitrogen cooled positive column discharge cell where a plasma is modulated at $\sim$ 40 kHz. The back reflected light is detected for PDH locking, and the transmitted light is used for heterodyne detection. The transmitted light is first demodulated by two mixers at $\sim$ 80 MHz and further demodulated by a pair of lock-in amplifiers at twice the plasma frequency. The resulting four channels of detection correspond to in-phase and quadrature detection from the lock-in amplifiers for each mixer.

Frequency calibration is performed either with a wavemeter or a frequency comb. The pump and signal beams are measured, and the idler frequency is determined by the difference of the pump and signal frequencies, shown in Equation 1. Here, f_i is the frequency of the idler, f_p is the frequency of the pump, and f_s is the frequency of the signal.

$$f_i = f_p - f_s \tag{1}$$

The inclusion of a frequency comb in this experiment is critical to lending unparalleled precision and accuracy to the determination of line centers. The improvement over ordinary wavemeters is drastic. Wavemeters tend to be accurate within 30 to 60 MHz, whereas sub-MHz precision and accuracy are typical with a frequency comb. Sub-MHz precision is critical to determining rotational spectra via combination differences. The requirement is a result of the intrinsically narrow linewidth of rotational lines.

Determination of a laser frequency with the comb is governed by Equation 2. In Equation

2, f is the frequency of the laser, n is the mode number of the frequency comb as determined by a wavemeter measurement, f_{rep} is the repetition rate of the comb, f_{ceo} is the carrier envelope offset, and f_{beat} is the frequency of the beat note of the laser against the comb. For the case of determining the idler frequency, Equation 1 is combined with Equation 2. The result is shown in Equation 3.

$$f = n(f_{rep}) \pm f_{ceo} \pm f_{beat} \tag{2}$$

$$f_i = (n_p - n_s) f_{rep} \pm f_{pbeat} \mp f_{sbeat} \tag{3}$$

In Equation 3, f_i is the idler frequency, n_p and n_s are the pump and signal modes determined by two wavemeter measurements, f_{pbeat} is the pump beat, and f_{sbeat} is the signal beat on the comb.

Scanning with the comb is accomplished by locking the pump to a comb mode and slewing the repetition rate of the comb. However, by changing the repetition rate, the signal beat is moved out of the bandpass region on the frequency counter during the scan. In order to remedy this, the signal light is coupled through an acousto-optic modulator (AOM) in a double pass configuration illustrated in Figure 2. The first order diffracted beam passes through the AOM twice leading to a shift in signal frequency of $2f_{AOM}$. This configuration is such that the pointing is independent of the AOM frequency. By shifting the frequency of the signal, the signal beat remains in the bandpass region of the frequency counter. When the extreme ranges of the AOM are reached, the frequency is reset and the signal mode number is incremented or decremented depending on the scan direction. Ultimately, the comb measures the $f_{sbeat} + 2f_{AOM}$, but the contribution by the AOM is subtracted in software before f_i is determined by Equation 3.

2. Testing via H_3^+ Spectroscopy

The instrument was first tested by measuring the R(1,0) and R(1,1)^u transitions of the ν_2 vibrational band of H_3^+. [8] H_3^+ was created in a pure hydrogen plasma by the electron ionization of a hydrogen molecule and the subsequent reaction with another hydrogen molecule.

$$\begin{aligned} H_2 + e^- &\rightarrow H_2^+ + 2e^- \\ H_2^+ + H_2 &\rightarrow H_3^+ + H \end{aligned} \tag{4}$$

H_3^+ is the most abundant molecular ion in a hydrogenic discharge. [15] The relative ease of production and abundance make it suitable testbed for the instrument.

The use of a high power light source and an optical cavity enable the saturation of rovibrational transitions. Spectroscopically, this phenomenon manifests as Lamb dips in the spectra. The NICE-OHVMS instrument observed Lamb dips for both R(1,0) and R(1,1)^u, shown in Figure 3. R(1,0) is shown in Figure 4. These are not the first Lamb dips to be observed for H_3^+, [16] but the they do represent the highest signal to noise Lamb dips of H_3^+ to date and, therefore, are easily fit to high precision for line center determination. An example fit may be seen in Figure 5. The full width at half maximum (FWHM) value for the Lamb dips is $\sim$ 60 MHz. Since the heterodyne frequency is on the order of the Lamb dip width and all the Lamb dips are blended together, it is difficult to make a precise statement about the FWHM.

The initial work was completed before the frequency comb was integrated into the instrument, but the precision associated with the fitting the R(1,0) Lamb dips was 70 kHz (the spectra from all four acquisition channels are simultaneously fit). Current work is underway to measure the transitions calibrated to a frequency comb. Early results indicate a statistical standard deviation of $\sim$ 400 kHz for line center determination, which supports the instrumental claim that line centers may be determined to sub-MHz precision.

The sensitivity of the instrument was determined to be 8.5×10^{-10} cm^{-1}Hz$^{-1/2}$, which corresponds to about two orders of magnitude above the shot noise limit for this particular system. Other fiber based lasers used in NICE-OHMS have similarly had sensitivities that were between one and two orders of magnitude away from the shot noise limit. This discrepancy is attributed to poor polarization matching to the EOM due to residual misalignments in the fiber production process.[17, 18]. This causes fiber based lasers to be especially sensitive to environmental factors.

B. Indirect Rotational Spectroscopy of HCO^+

As a testbed for determining a rotational spectrum indirectly, the cavity was removed and the instrument was used in a single pass configuration. The second attached paper describes this work. [19] Without a counter propagating beam, sub-Doppler spectroscopy is not possible. Therefore, Doppler broadened lines of HCO^+ were observed instead. The

P(10) through R(9) lines of the ν_1 fundamental band were all comb calibrated and fit to determine the line centers. The line centers were compared to the previous work by Amano. [20] The average signal to noise was $\sim$ 300 for the more intense lines and $\sim$ 100 for the least intense lines. The statistical precision on the line center determination was $\sim$ 600 kHz. Combination differences were calculated for the ground state and $1\nu_1$ excited state. The largest error compared to the known ground state rotational spectra [1] was 2.5 MHz. By using the J = 3 $\leftarrow$ 2 transition in the $1\nu_1$ state [21], the entire excited rotational spectrum was determined with an average error of $\sim$ 2 MHz, which is well within a reasonable window for a direct rotational search. The band origin was determined to be ν = 3088.739009(5) cm^{-1}, and the excited state rotational constants B_1 = 44240.536(9) MHz and D_1 = 82.31(9) kHz were determined. This work is a clear demonstration of how combination differences can be used to calculate rotational spectra.

III. PROPOSED WORK

Highly fluxional species are molecules with large amplitude internal motions. In general, these molecules may be considered as having saddle points that are close to the minimum potential energy relative to the zero point energy. These saddle points have significant wavefunction amplitude, which suggests that the molecules are, in classical terms, undergoing near constant motion through these low energy pathways.

Two examples of fluxional molecules with five equivalent atoms are addressed herein, CH_5^+ and H_5^+. CH_5^+ can undergo a flip motion and internal rotation. [22, 23] Whereas, H_5^+ has 9 conformations all within $\sim$ 2800 cm^{-1} of the minimum, demonstrating the relative ease with which this molecule may change conformation. [24]

A. CH_5^+ Spectroscopy

The molecular ion CH_5^+ was first observed via high resolution infrared spectroscopy by White *et al.* [25] There were 917 lines observed belonging to the ion between 2770 and 3150 cm^{-1}. However, it remains unassigned due to the fluxional nature of the molecule. The potential energy surface has two saddle points that exist at low energies and have significant wavefunction amplitude in the ground state. Classically, it is analogous to the protons

continuously scrambling around the carbon atom. There are 5! = 120 equivalent minima with C_s symmetry, there are 120 saddle points that correspond to the internal rotation $\sim$ 40 cm^{-1} above the global minimum, and there are 60 saddle points that correspond to the flip motion $\sim$ 300 cm^{-1}above the global minimum. [26]

The most accurate work to date is a numerically exact 12 dimensional calculation of the vibrational energy levels. [26] However, it makes no consideration of rotation so it cannot represent actual transitions of CH_5^+. The interesting result from this work is that the potential energy surface is modified by creating a "floor" that is used to fill the low level energy structures. The calculations found that the pattern in vibrational frequencies did not change significantly, which seems to suggest that these structures are insignificant to the overall spectral pattern related to vibrational energy levels.

There has also been considerable work completed in determining the millimeter-wave spectrum of CH_5^+. The most recent work was by Bunker *et al.* [27] wherein a rotational spectrum was calculated by considering the flip and internal rotation coordinates solely. Though the range in which the $J = 1 \leftarrow 0$ rotation transition is predicted to occur is too large to be useful(15 GHz), the overall structure may be similar to what is observed by performing a combination differences analysis.

1. Four-line Combination Differences Analysis

Using the NICE-OHVMS spectrometer, the 917 observed lines of CH_5^+ will be revisited using high precision spectroscopy. CH_5^+ is produced in a hydrogen dominated plasma with methane. The reaction of H_3^+ with CH_4 is the most significant production path. [25].

$$CH_4 + H_3^+ \rightarrow H_2 + CH_5^+ \tag{5}$$

Initial observations have been made but they are not instrumentally optimized. Figures 6 and 7 show these spectra. Currently, we are limited by absorption in the cavity mirrors due to water in the dielectric coating. Nevertheless, after the optimum signal is achieved, the transitions can be measured with unprecedented accuracy.

Frequency comb calibrating the scans and fitting Lamb dips for each transition will result in a significant advancement in the field. The most exciting analysis of these high precision lines that can be performed is a combination difference calculation. When such an analysis

is done on a molecule with known rotational structure, the rotational spectrum can be calculated. This is not the case with CH_5^+. This particular ion has never had a rotational spectrum observed. For this reason, four-line combination differences are necessary.

An ordinary combination difference is calculated between two transitions that share a known state. Without *a priori* knowledge of the rovibrational structure, a single combination difference is useless for determining energy level spacings. However, if there exists a pair of combination differences that match, the energy level spacing is a valid rotational energy level spacing.

After determining all of the values of the energy levels from these unassigned lines, a pattern may emerge, which is a real experimental advance. It is important to note that this will not provide an assignment, but may provide insight into the underlying structure.

2. Discovery Spectroscopy

The spectrum of CH_5^+ has been observed at low resolution using an ion trap and a free electron laser.[28] Laser induced reaction spectroscopy was performed and three bands were observed. The band centered at 1250 cm^{-1} corresponds to a C-H bend and has never been observed with high resolution.[29]

Progress is being made on the development of an external cavity quantum cascade laser (EC-QCL) ringdown experiment, which is expected to be tunable from 1140 to 1250 cm^{-1}. The band that is centered at 1250 cm^{-1} has significant overlap with the expected coverage of the EC-QCL, which will make it a logical choice for a high resolution line search of CH_5^+.

A liquid nitrogen cooled positive column discharge cell can be placed within a cavity and aligned for ringdown. Typical cavity ringdown experiments have sensitivities of $\sim 1 \times 10^{-9}$ cm^{-1}, which is comparable to the sensitivities achieved with the current detector, mirrors, and QCL in use.[30] Assuming the coupling efficiency is not drastically different, similar sensitivities may be achieved. The only new source of noise would be the electronic noise associated with the plasma. The band observed previously is 3/5 the intensity of the most intense band after normalizing the intensity for the rate of reaction. [28] The most intense transition reported by Oka has been observed with the NICE-OHVMS instrument described above (Figures 6 and 7), which has a similar sensitivity to the QCL instrument. Therefore, it is not unreasonable to assume that some new lines may be resolved out of the band.

B. Discovery Spectroscopy of H_5^+

H_5^+ is a highly fluxional molecule that has not yet been observed with high resolution spectroscopy. Diffusion Monte Carlo (DMC) and variational techniques have been used to assign vibrational modes to observed multi-photon dissociation spectra.[31, 32]. These works have illustrated that the exchange of the proton is a high intensity mode. The very high intensity mode is due to the large change in dipole associated with a moving charge as is expected, but the exact vibrational energies associated with these methods may not be entirely accurate. Using DMC for excited states rather than the ground state assumes *a priori* knowledge of the excited state nodal structure. [33] This approach can be inaccurate due to the sensitivity of the answer to the assumptions that go into the calculation. Variational techniques require the choice of a reference geometry, which is difficult when dealing with fluxional molecules.

These theoretical challenges, however, do not diminish the importance of the multi-photon dissociation work. There are many bands that have been observed in a recent publication by Cheng *et al.* [32]. Most importantly, there exists a band centered at 1180 cm^{-1}, which is within the coverage of the EC-QCL system. It appears to be a low intensity band, but it is important to consider that intensities are more or less meaningless for multi-photon dissociation. Multi-photon dissociation spectroscopy relies on the fortuitous alignment of photon energies with transitions up until the dissociation energy is reached, and the molecule is destroyed. These fortuitous alignments may or may not overlap with transitions, which affects the observed intensity of the band. In a purely harmonic system, the intensity would be significant because the observed intensity would simply be normalized against the number of photons that were absorbed. However, H_5^+ is very anharmonic and the intensities displayed bear little relevance to the intensity of an absorption feature. [32] Additionally, the exact band centers may not correspond perfectly to the band center of an absorption spectrum. Enhanced resonance may not occur precisely peaked at the center of the band, instead relying on the density of states to help match the ideal route to dissociation.

This molecular ion is formed in a hydrogenic plasma via the clustering of H_3^+ with a hydrogen molecule.

$$H_3^+ + H_2 + H_2 \rightarrow H_5^+ + H_2 \tag{6}$$

The reactant species in Equation 6 are the most common species in a hydrogen plasma

so production is feasible. H_5^+ has been experimentally inferred by observing a reduction at higher pressures of the intensity of H_3^+ transitions. [34] This reaction to produce H_5^+ relies on three-body collisions to remove the excess energy of the H_5^+ complex. The removal of excess energy allows the ion to stabilize below its dissociation energy. Therefore, the production proceeds more favorably at higher pressures. A hollow cathode can achieve colder temperatures when cooled with liquid nitrogen and higher pressures as compared to a positive column. These facts make it a better choice for the production of H_5^+. [34] By using the EC-QCL system with a hollow cathode, a line search may be conducted. New transitions that can be attributed to H_5^+ may be observed with rotational resolution for the first time, which would be a boon to understanding this fluxional molecular ion. By providing theorists with a target spectrum, numerical calculations similar to the work accomplished by Wang *et al.* [26] may be undertaken.

IV. SUMMARY

The first mid-IR NICE-OHVMS spectrometer has been constructed. It made its debut with sub-Doppler spectroscopy of H_3^+, and the resultant Lamb dips were fit to sub-MHz precision and accuracy, demonstrating the utility of the instrument. The quality of combination differences using this instrument was assessed via Doppler broadened HCO^+ spectroscopy. The results were used to implement indirect rotational spectroscopy.

Four-line combination differences are proposed for the 917 previously observed transitions between 2770 and 3150 cm^{-1}. It is hoped that information regarding the underlying structure of CH_5^+ can be gained. Using an EC-QCL, line searches are to be conducted for CH_5^+ and H_5^+ in the 1140 to 1250 cm^{-1} region, discovering new transitions belonging to these species to guide theory.

---

[1] G. Cazzoli, L. Cludi, G. Buffa, C. Puzzarini, "Precise THz Measurements of HCO^+ , N_2H^+ , and CF^+ for Astrophysical Observations" *Astrophys. J. Suppl. S.* (2012), **203**(1), 11.

[2] D. Buhl, L. E. Snyder, "Unidentified interstellar microwave line." *Nature* (1970), **228**(5268), 267–9.

[3] R. Woods, T. Dixon, R. Saykally, P. Szanto, "Laboratory Microwave Spectrum of HCO^+" *Phys. Rev. Lett.* (1975), **35**(19), 1269–1272.

[4] C. Sanchez Contreras, R. Sahai, "Physical Structure of the Protoplanetary Nebula CRL 618. II. Interferometric Mapping of a Millimeter-wavelenght HCN J = 1-0, HCO^+ J = 1-0, and Continuum Emission" *Astrophys. J.* (2004), **602**(2), 960–977.

[5] C. R. Purcell, R. Balasubramanyam, M. G. Burton, a. J. Walsh, V. Minier, M. R. Hunt-Cunningham, L. L. Kedziora-Chudczer, S. N. Longmore, T. Hill, I. Bains, P. J. Barnes, a. L. Busfield, P. Calisse, N. H. M. Crighton, S. J. Curran, T. M. Davis, J. T. Dempsey, G. Derragopian, B. Fulton, M. G. Hidas, M. G. Hoare, J.-K. Lee, E. F. Ladd, S. L. Lumsden, T. J. T. Moore, M. T. Murphy, R. D. Oudmaijer, M. B. Pracy, J. Rathborne, S. Robertson, a. S. B. Schultz, J. Shobbrook, P. a. Sparks, J. Storey, T. Travouillion, "A CH_3CN and HCO+ survey towards southern methanol masers associated with star formation" *Mon. Not. R. Astron. Soc.* (2006), **367**(2), 553–576.

[6] S. N. Milam, C. Savage, L. M. Ziurys, S. Wyckoff, "HCO^+ Observations toward comet Hale-Bopp (C/1995 O1): Ion-molecule Chemistry and Evidence for a Volatile Secondary Source" *Astrophys. J.* (2004), **615**(2), 1054–1062.

[7] H. Liszt, R. Lucas, "Mm-wave HCO^+, HCN and CO absorption toward NGC 1052" *Astron. Astrophys.* (2004), **428**(2), 445–450.

[8] K. N. Crabtree, J. N. Hodges, B. M. Siller, A. J. Perry, J. E. Kelly, P. A. Jenkins, B. J. McCall, "Sub-Doppler mid-infrared spectroscopy of molecular ions" *Chem. Phys. Lett.* (2012), **551**, 1–6.

[9] B. M. Siller, M. W. Porambo, A. A. Mills, B. J. McCall, "Noise immune cavity enhanced optical heterodyne velocity modulation spectroscopy." *Opt. Express* (2011), **19**(24), 24822–7.

[10] C. Gudeman, M. Begemann, J. Pfaff, R. Saykally, "Velocity-Modulated Infrared Laser Spectroscopy of Molecular Ions: The ν_1 Band of HCO^+" *Phys. Rev. Lett.* (1983), **50**(10), 727–731.

[11] S. K. Stephenson, R. J. Saykally, "Velocity modulation spectroscopy of ions." *Chem. Rev.* (2005), **105**(9), 3220–34.

[12] C. S. Gudeman, R. J. Saykally, "Velocity Modulation Infrared Laser Spectroscopy of Molecular Ions" *Annu. Rev. Phys. Chem.* (1984), **35**(1), 387–418.

[13] L.-S. Ma, J. Ye, P. Dubé, J. L. Hall, "Ultrasensitive frequency-modulation spectroscopy enhanced by a high-finesse optical cavity: theory and application to overtone transitions of C_2H_2

and C_2HD" *J. Opt. Soc. Am. B* (1999), **16**(12), 2255.

[14] A. Foltynowicz, F. Schmidt, W. Ma, O. Axner, "Noise-immune cavity-enhanced optical heterodyne molecular spectroscopy: Current status and future potential" *Appl. Phys. B* (2008), **92**(3), 313–326.

[15] T. Oka, "Observation of the Infrared Spectrum of H_3^+" *Phys. Rev. Lett.* (1980), **45**(7), 531–534.

[16] H.-C. Chen, C.-Y. Hsiao, J.-L. Peng, T. Amano, J.-T. Shy, "High-Resolution Sub-Doppler Lamb Dips of the ν_2 Fundamental Band of H_3^+" *Phys. Rev. Lett.* (2012), **109**(26), 263002.

[17] P. Ehlers, I. Silander, J. Wang, O. Axner, "Fiber-laser-based noise-immune cavity-enhanced optical heterodyne molecular spectrometry instrumentation for Doppler-broadened detection in the $10^{-12} cm^{-1} Hz^{-1/2}$ region" *J. Opt. Soc. Am. B* (2012), **29**(6), 1305.

[18] A. Foltynowicz, I. Silander, O. Axner, "Reduction of background signals in fiber-based NICE-OHMS" *J. Opt. Soc. Am. B* (2011), **28**(11), 2797.

[19] B. M. Siller, J. N. Hodges, A. J. Perry, B. J. McCall, "Indirect rotational spectroscopy of HCO^+" (2013), *J. Phys. Chem. A*, Submitted.

[20] T. Amano, "The ν_1 fundamental band of HCO^+ by difference frequency laser spectroscopy" *J. Chem. Phys.* (1983), **79**(7), 3595.

[21] V. Lattanzi, A. Walters, B. J. Drouin, J. C. Pearson, "Rotational Spectrum of the Formyl Cation, HCO^+ , to 1.2 THz" *Astrophys. J.* (2007), **662**(1), 771–778.

[22] M. Kolbuszewski, P. R. Bunker, "Potential barriers, tunneling splittings, and the predicted J=1←0 spectrum of CH_5^+" *J. Chem. Phys.* (1996), **105**(9), 3649.

[23] A. L. L. East, M. Kolbuszewski, P. R. Bunker, "Ab Initio Calculation of the Rotational Spectrum of CH_5^+ and CD_5^+" *J. Phys. Chem. A* (1997), **101**(36), 6746–6752.

[24] Y. Yamaguchi, J. F. Gaw, R. B. Remington, H. F. Schaefer, "The H_5^+ potential energy hypersurface: Characterization of ten distinct energetically low-lying stationary points" *J. Chem. Phys.* (1987), **86**(9), 5072.

[25] E. T. White, J. Tang, T. Oka, "CH_5^+: The Infrared Spectrum Observed" *Science* (1999), **284**(5411), 135–137.

[26] X.-G. Wang, T. Carrington, "Vibrational energy levels of CH_5^+" *J. Chem. Phys.* (2008), **129**(23), 234102.

[27] P. Bunker, B. Ostojić, S. Yurchenko, "A theoretical study of the millimeterwave spectrum of CH_5^+" *J. Mol. Struct.* (2004), **695-696**, 253–261.

[28] O. Asvany, P. Kumar P, B. Redlich, I. Hegeman, S. Schlemmer, D. Marx, "Understanding the Infrared Spectrum of Bare CH_5^+" *Science* (2005), **309**(5738), 1219–1222.

[29] X. Huang, A. McCoy, J. Bowman, L. Johnson, C. Savage, F. Dong, D. Nesbitt, "Quantum Deconstruction of the Infrared Spectrum of CH_5^+" *Science* (2006), **311**(5757), 60–63.

[30] B. E. Brumfield, J. T. Stewart, S. L. Widicus Weaver, M. D. Escarra, S. S. Howard, C. F. Gmachl, B. J. McCall, "A quantum cascade laser cw cavity ringdown spectrometer coupled to a supersonic expansion source." *Rev. Sci. Instrum.* (2010), **81**(6), 063102.

[31] T. C. Cheng, B. Bandyopadyay, Y. Wang, S. Carter, B. J. Braams, J. M. Bowman, M. a. Duncan, "Shared-Proton Mode Lights up the Infrared Spectrum of Fluxional Cations H_5^+ and D_5^+" *J. Phys. Chem. Lett.* (2010), **1**(4), 758–762.

[32] T. C. Cheng, L. Jiang, K. R. Asmis, Y. Wang, J. M. Bowman, A. M. Ricks, M. A. Duncan, "Mid- and Far-IR Spectra of H_5^+ and D_5^+ Compared to the Predictions of Anharmonic Theory" *J. Phys. Chem. Lett.* (2012), **3**(21), 3160–3166.

[33] Z. Lin, A. B. McCoy, "Signatures of Large-Amplitude Vibrations in the Spectra of H_5^+ and D_5^+" *J. Phys. Chem. Lett.* (2012), **3**(24), 3690–3696.

[34] K. N. Crabtree, C. A. Kauffman, B. A. Tom, E. Beçka, B. A. McGuire, B. J. McCall, "Nuclear spin dependence of the reaction of H_3^+ with H_2. II. Experimental measurements." *J. Chem. Phys.* (2011), **134**(19), 194311.

Figures

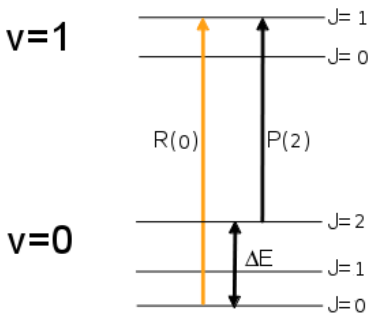

FIG. 1: Illustration of the determination of the rotational energy level spacing, $\Delta E_{J=2\leftarrow 0}$, by combination difference.

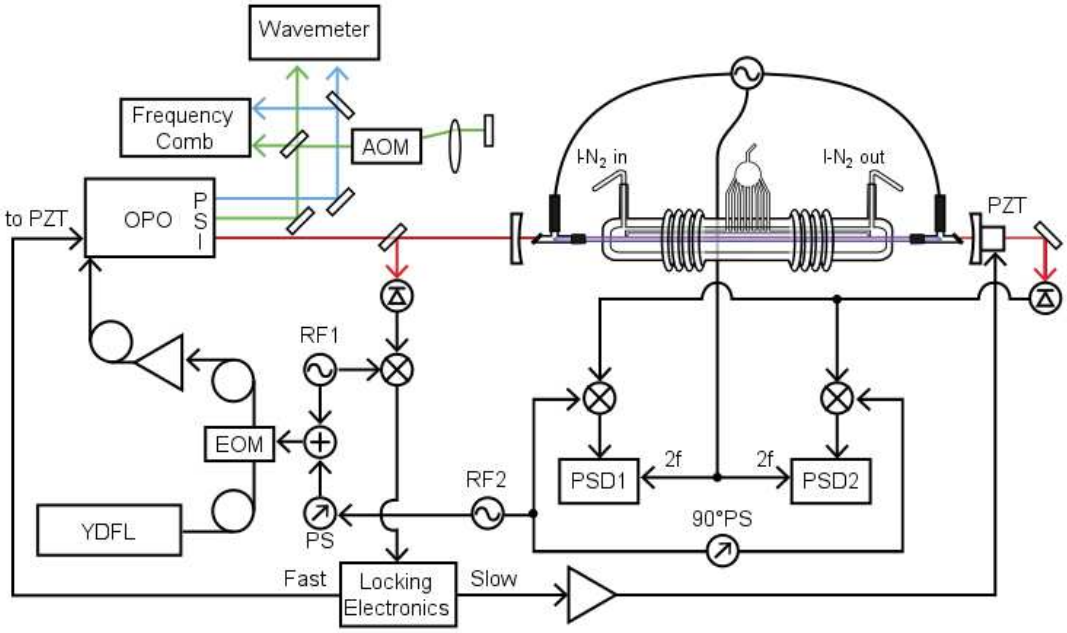

FIG. 2: A block diagram of the instrument. (YDFL: Ytterbium Doped Fiber Laser, EOM: Electro-optic Modulator, OPO: Optical Parametric Oscillator, P: Pump, S: Signal, I: Idler, PZT: Piezo Tranducer, PSD: Phase Sensitive Detector, RF: Radio Frequency Generator, PS: Phase Shifter, AOM: Acousto-optic Modulator)

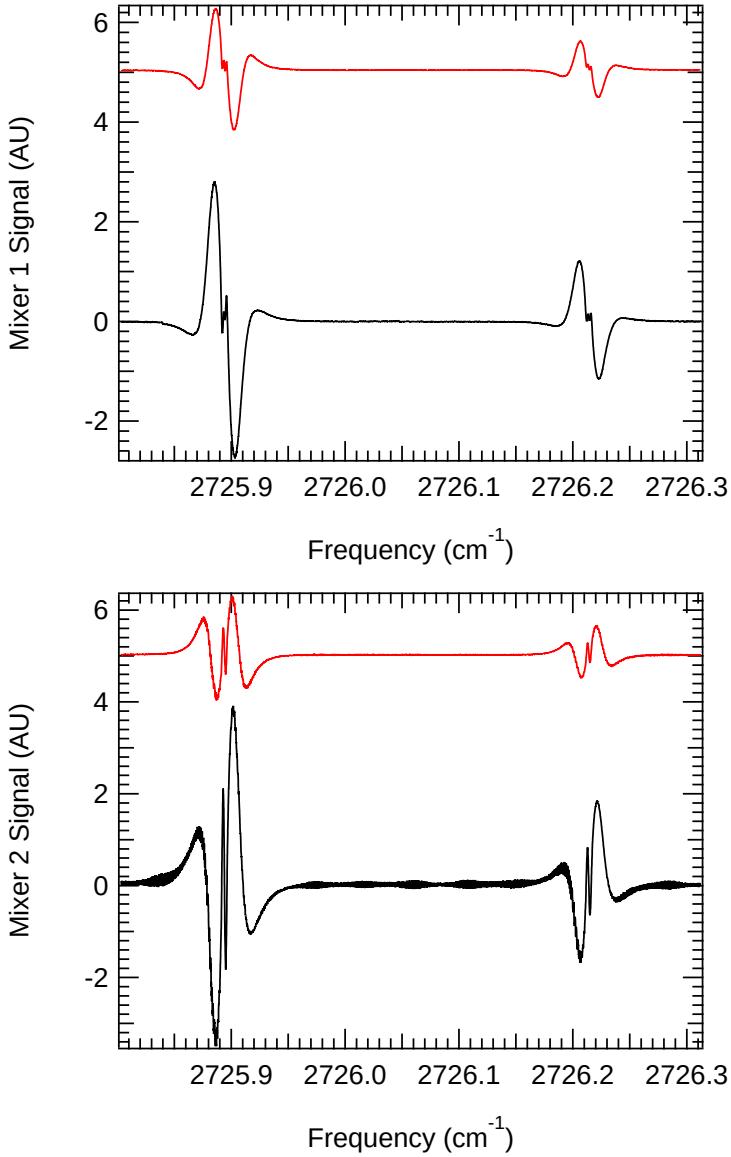

FIG. 3: This is a continuous scan that covers the R(1,0) and R(1,1)^u lines of H_3^+. All four channels are displayed. Black corresponds to in-phase detection with the lock-in amplifiers, whereas red corresponds to the quadrature detection of the lock-in amplifiers. Adapted from attached paper (Ref. [8])

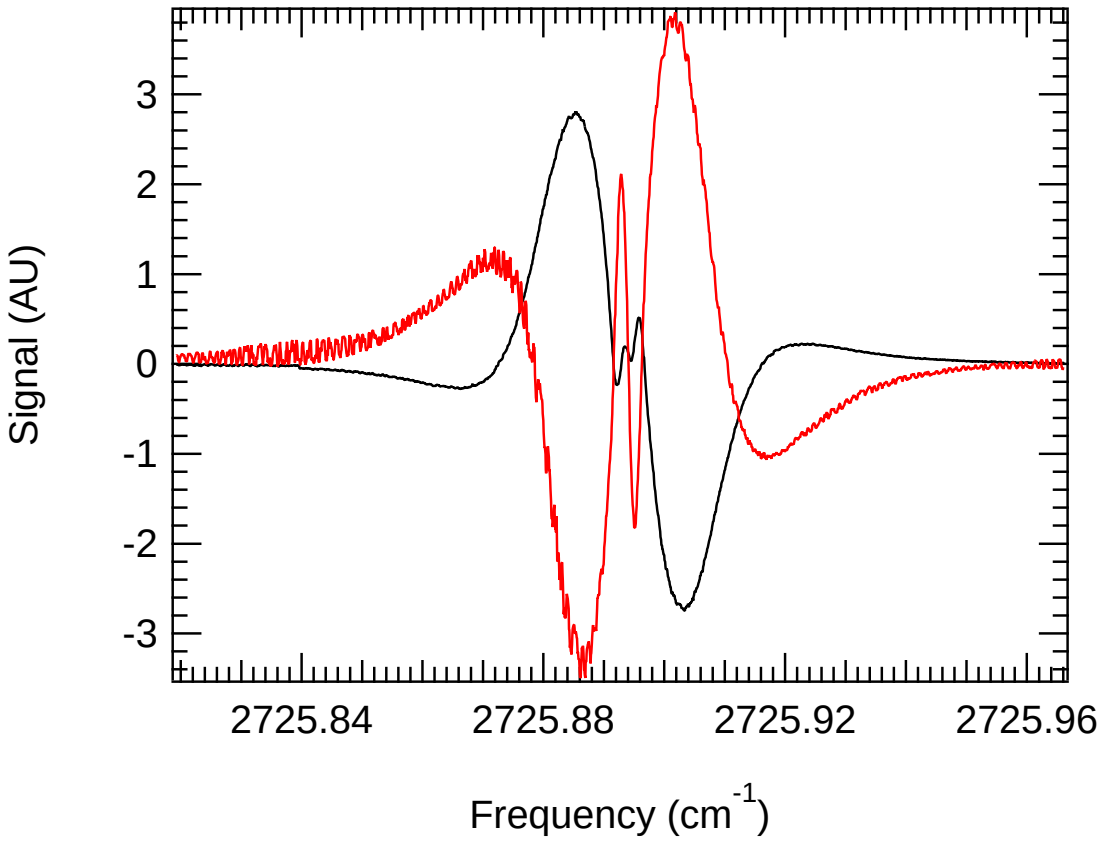

FIG. 4: A smaller scan showing the output of mixer 1. Black corresponds to in-phase detection with the lock-in amplifiers, whereas red corresponds to the quadrature detection of the lock-in amplifiers.Adapted from attached paper (Ref. [8])

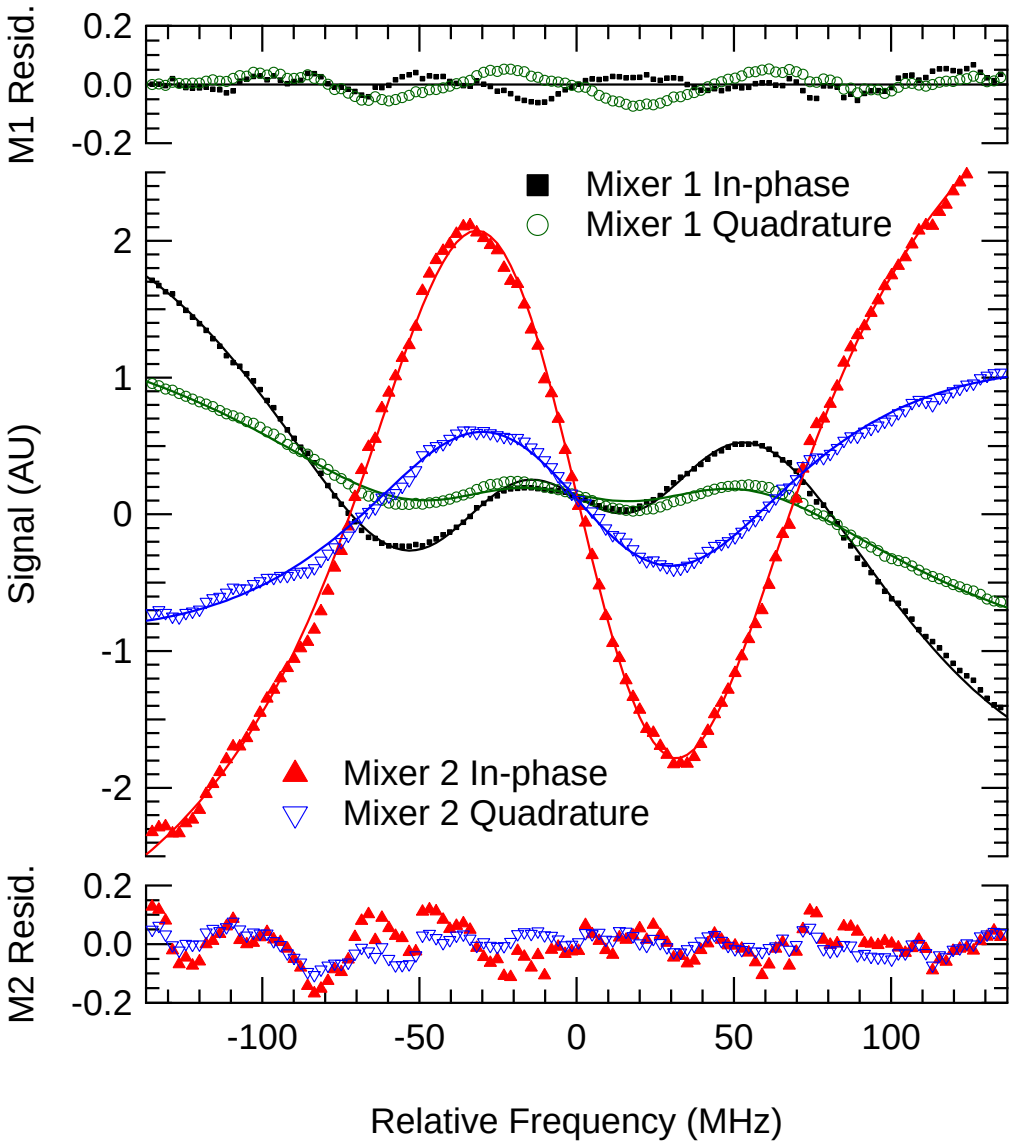

FIG. 5: Zoomed in fit of Lamb dips. The output of all four channels is displayed and the residuals are plotted according to which mixer they correspond. The in-phase and quadrature detection corresponds to the phase of the lock-in amplifiers. Adapted from attached paper (Ref. [8])

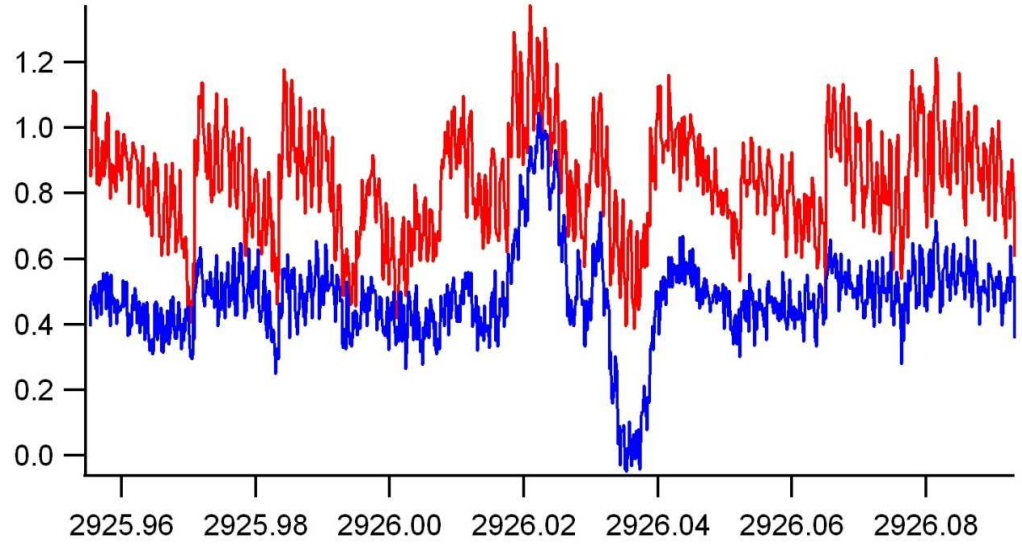

FIG. 6: Preliminary scan of CH_5^+. Output from mixer 1. The red trace is the in-phase detection the blue trace is the quadrature detection. There may be a hint of a Lamb dip in the quadrature channel.

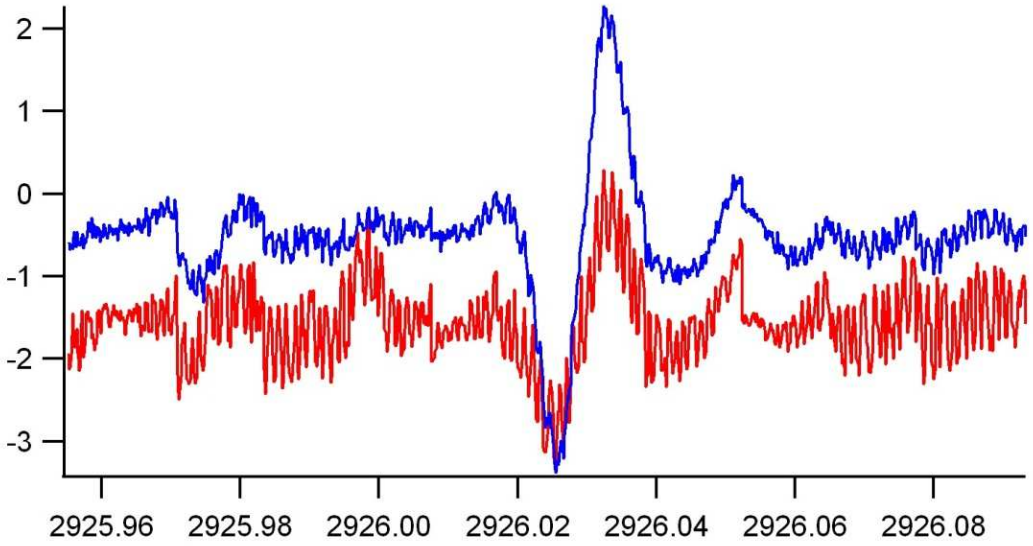

FIG. 7: Preliminary scan of CH_5^+. Output from mixer 2. The red trace is the in-phase detection the blue trace is the quadrature detection.

Chemical Physics Letters 551 (2012) 1–6

Contents lists available at SciVerse ScienceDirect

Chemical Physics Letters

journal homepage: www.elsevier.com/locate/cplett

FRONTIERS ARTICLE

Sub-Doppler mid-infrared spectroscopy of molecular ions

Kyle N. Crabtree [a,1], James N. Hodges [a], Brian M. Siller [a], Adam J. Perry [a], Joseph E. Kelly [a], Paul A. Jenkins II [a], Benjamin J. McCall [a,b,*]

[a] Department of Chemistry, University of Illinois, Urbana, IL 61801, USA
[b] Departments of Astronomy and Physics, University of Illinois, Urbana, IL 61801, USA

ARTICLE INFO

Article history:
Available online 15 September 2012

ABSTRACT

The technique of velocity modulation spectroscopy has recently been combined with cavity enhancement and frequency modulation methods into a technique called noise-immune cavity-enhanced optical heterodyne velocity modulation spectroscopy (NICE-OHVMS). We have implemented NICE-OHVMS with a cw-optical parametric oscillator (OPO) tunable from 3.2 to 3.9 μm, and used it to record spectra of the $R(1,0)$ and $R(1,1)^u$ transitions of the v_2 fundamental band of H_3^+. The high optical power and cavity enhancement enable saturation of rovibrational transitions, which allows for line center frequencies to be measured with a precision of 70 kHz.

1. Introduction

Molecular ions play a key role as intermediates in chemical reactions, and a detailed understanding of their structure and intramolecular dynamics in the gas phase, generally obtained by spectroscopy, is a critical first step toward understanding their behavior in more complicated systems. The primary technique used for ion spectroscopy over the past 30 years has been velocity modulation spectroscopy (VMS) [1,2]. In VMS, ions are produced in an AC positive column plasma whose polarity is alternated at frequency f_{vm}. The average drift velocity of the ions in the plasma is shifted toward the cathode from the applied electric field, while neutral molecules are generally unaffected. As the polarity is reversed, the average ion drift velocity also reverses, resulting in a periodic oscillation in the ion velocity distribution at f_{vm}. By interrogating the ions with a laser beam passing in one direction through the plasma, the absorption profiles are alternately red- and blue-shifted with respect to their rest frequencies, and phase-sensitive detection at f_{vm} allows for selective retrieval of ionic signals. VMS therefore addresses one of the main challenges of ion spectroscopy, i.e., detection of ionic species that are only $\sim 10^{-5}$–10^{-6} as abundant as neutral molecules. Well over 40 unique molecular ions (not including isotopologues) have been detected with VMS; these have been extensively reviewed by Stephenson and Saykally [3].

Recently, the use of a Fabry–Perot optical cavity to enhance the optical path length was demonstrated by Siller et al. (cavity-enhanced velocity modulation spectroscopy, CEVMS), who locked a Ti:Sapphire laser to an optical cavity surrounding a velocity modulated positive column cell and detected the transmitted light [4]. Because the light in the cavity is bidirectional, red and blue Doppler shifts are simultaneously superimposed, encoding the velocity modulation (VM) signal at $2f_{vm}$. Initially, this was believed to be problematic because any neutral molecules produced or excited by the discharge are concentration modulated (CM) at $2f_{vm}$; that is, the population of the excited species varies with the magnitude of the applied voltage, but not the sign of the voltage. By also encoding the ion signal at $2f_{vm}$, it was thought the concentration modulation signal of neutral molecules would overwhelm the ion velocity modulation signal. Siller et al. showed that the ion and neutral signals occurred at different phases with respect to the plasma voltage, thereby preserving ion-neutral discrimination through phase-sensitive detection. Additionally, the power enhancement from the optical cavity enables saturation spectroscopy and precise line-center determination [5]. A related technique has also been employed using an optical frequency comb as the light source and a unidirectional ring cavity surrounding a plasma cell, effectively converting VMS to a broadband technique while preserving the high resolution of laser spectroscopy [6].

Cavity enhanced absorption spectroscopy suffers from the fact that frequency noise in the laser is directly converted into intensity noise as a result of reduced cavity transmission. This limitation was overcome by Ye et al. with noise-immune cavity-enhanced

* Corresponding author at: Department of Chemistry, University of Illinois, Urbana, IL 61801, USA.
E-mail addresses: kcrabtr2@illinois.edu (K.N. Crabtree), jnhodge@illinois.edu (J.N. Hodges), bsiller2@illinois.edu (B.M. Siller), aperry10@illinois.edu (A.J. Perry), bjmccall@illinois.edu (B.J. McCall).
URL: http://bjm.scs.illinois.edu (B.J. McCall).
[1] Present address: Harvard-Smithsonian Center for Astrophysics, Cambridge, MA 02138, USA.

0009-2614/$ - see front matter © 2012 Elsevier B.V. All rights reserved.
http://dx.doi.org/10.1016/j.cplett.2012.09.015

optical heterodyne molecular spectroscopy (NICE-OHMS) [7]. In this technique, the laser is phase modulated at f_h (typically ~100s of MHz), effectively generating an FM triplet consisting of a carrier (at the optical frequency f_o) and a pair of sidebands with opposite phase at $f_o \pm f_h$. The triplet is coupled into the optical cavity by setting f_h equal to an integer multiple of the cavity free spectral range (FSR). In the absence of any intracavity absorption or dispersion, the beat notes between each sideband beating with the carrier are balanced in both amplitude and phase, so there is no net signal at f_h. However, in the presence of an intracavity absorber or disperser, the beat notes are unbalanced in amplitude and/or phase, yielding a net signal. By encoding absorption/dispersion information at a high frequency, $1/f$ technical noise is reduced. Another advantage is that any laser frequency noise affects the cavity coupling efficiency of the carrier and both sidebands equally, which keeps the beat notes of each sideband with the carrier balanced, and eliminates direct conversion of laser frequency noise to noise in the final spectrum. The disadvantages are the complexity of the technique, particularly the demands of maintaining the laser-cavity lock, and the requirement of a detector whose bandwidth is at least f_h. An extensive review of the NICE-OHMS technique has been published by Foltynowicz et al. [8].

CEVMS and NICE-OHMS have been combined into a technique called noise-immune cavity enhanced optical heterodyne velocity modulation spectroscopy (NICE-OHVMS) in the near-infrared with a Ti:Sapphire laser [9]. Because f_h and f_{vm} are at significantly different frequencies (typically ~100 MHz and ~10 kHz, respectively), the detector signal is first demodulated at f_h, and then sent on to further phase-sensitive detection at $2f_{vm}$. NICE-OHVMS preserves the ion-neutral discrimination afforded by VMS, and takes advantage of the ultra-high sensitivity, saturation, and noise immunity of NICE-OHMS.

However, the technical demands of the NICE-OHMS technique have largely precluded its use in the mid-infrared spectral region in which VMS has been successfully exploited. The high bandwidth detectors and phase modulators required for NICE-OHMS are not as readily available in the mid-IR compared with the visible/near-IR. The only published mid-IR NICE-OHMS work was done with a quantum cascade laser near 8.5 μm, and was limited by the detector bandwidth and the phase modulation characteristics of the device [10]. Work is currently underway in our laboratory to extend NICE-OHMS into the mid-IR using a difference frequency generation (DFG) source in the 3–5 μm region [11], which is particularly attractive for a general-purpose ion spectrometer because the vast majority of molecules have at least one fundamental vibrational band in that portion of the spectrum.

Here we report the first mid-IR NICE-OHVMS spectrometer, which uses a commercially available cw-optical parametric oscillator (OPO) tunable from 3.2 to 3.9 μm. The high optical power of the OPO (~1 W) allows for use of high bandwidth mid-IR detectors that are not sensitive enough to be used with many other lower-power cw lasers in this region. This technique enables all of the advantages of the NICE-OHVMS technique to be brought to bear on fundamental vibrational transitions of molecular ions, including high precision sub-Doppler spectroscopy.

Our initial demonstration of this instrument focuses on the study of H_3^+, which is the simplest polyatomic molecular ion and serves as the primary initiator of ion–molecule chemistry in interstellar clouds [12,13]. Its infrared spectrum was first observed by Oka in 1980 [14], and since then it has been extensively studied spectroscopically (see, for instance, the review in Ref. [15]). More recent research on H_3^+ focuses on spectroscopy above the so-called "barrier to linearity," at which point the molecule adopts a linear geometry that induces a singularity in the Hamiltonian, complicating its theoretical treatment [16]. Nevertheless, for the lowest-lying energy levels, the agreement between experiment and ab initio theory is good to spectroscopic accuracy [17]. Measuring the energy level spacings experimentally with higher precision and accuracy would present a greater challenge for ab initio theory, possibly spurring new developments. The NICE-OHVMS technique opens the possibility of measuring such energy level spacings in H_3^+.

As a demonstration of the capabilities of this instrument, we present in this Letter spectra of the ν_2 fundamental band of H_3^+ at 3.67 μm. In Section 2 we describe the instrumental details, and in Section 3 we discuss NICE-OHVMS lineshapes and present spectra acquired with the instrument. Finally, in Section 4, the performance of the instrument is assessed, and future directions are discussed.

2. Experimental details

Our NICE-OHVMS instrument is outlined in Figure 1. A Ytterbium-doped fiber laser (YDFL, Koheras Adjustik Y-10) is sent through a fiber EOM (EOSPACE PM-0K5–00-PFU-PFU-106-S), amplified (IPG Photonics YAR-10 K-1064-LP-SF), and used to pump a singly-resonant OPO (Aculight Argos 2400 SF). The pump (1.064 μm) and signal (1.5–1.6 μm) beams are sent to a wavemeter (Burleigh WA-1500) for frequency calibration. The idler (3.2–3.9 μm) is locked with the Pound-Drever-Hall (PDH) technique to a 1.9-m-long optical cavity consisting of two 1 m radius of curvature concave Si mirrors dielectric coated for 99.7% reflectivity over 3.1–3.4 μm surrounding a plasma cell. Cavity reflection and transmission are monitored by photodiodes (Boston Electronics Vigo PVM-10.6-1x1) with an effective bandwidth of ~125 MHz.

Heterodyne and PDH sidebands are generated by applying voltages at their respective frequencies to the fiber EOM on the seed laser simultaneously. The resultant frequency spectrum of the pump laser is imprinted on the idler beam. A PDH error signal used for cavity locking is generated by demodulating the cavity reflection signal at the frequency RF1 (typically 2–20 MHz). The error signal is sent to feedback electronics which stabilize the length of the cavity on slow timescales via a piezoelectric transducer (PZT) attached to one of the cavity mirrors, and apply fast corrections to the idler frequency by a PZT mounted to one of the signal cavity mirrors inside the OPO head. The cavity transmission detector signal is sent to a pair of mixers ~90° out of phase with one another, and each is demodulated at frequency RF2 (equal to the cavity FSR of 79.12 MHz). The overall phase of the heterodyne detection is adjusted by phase shifting the RF signal driving the EOM using cables of appropriate lengths. The demodulated signal from each mixer is then sent to a lock-in amplifier referenced to twice the frequency used to drive the plasma, and the in-phase and quadrature outputs of each amplifier are digitized and stored on a computer.

Ions are produced in a liquid-nitrogen-cooled multi-inlet multi-outlet positive column discharge cell, which is placed between the two free-standing mirrors of the optical cavity [18]. Intracavity radiation is admitted into the cell by means of CaF_2 windows aligned at Brewster's angle. The plasma is driven by a 40 kHz sine wave voltage produced by amplifying the output of an arbitrary waveform generator with an audio amplifier (Techron 7780) and a step-up transformer. H_3^+ was produced at a pressure of 200 mTorr and a discharge current of 170 mA. The outputs of the two mixers were each demodulated at 80 kHz with a lock-in amplifier set to a 10 ms time constant (16 Hz detection bandwidth).

Typical operation begins by filling the cooling jacket of the cell with liquid nitrogen and igniting the plasma. The cavity length is adjusted to bring it into resonance with the laser, and the laser-cavity lock is established. The idler frequency is tuned by applying a voltage to an internal PZT on the YDFL, and the cavity length is

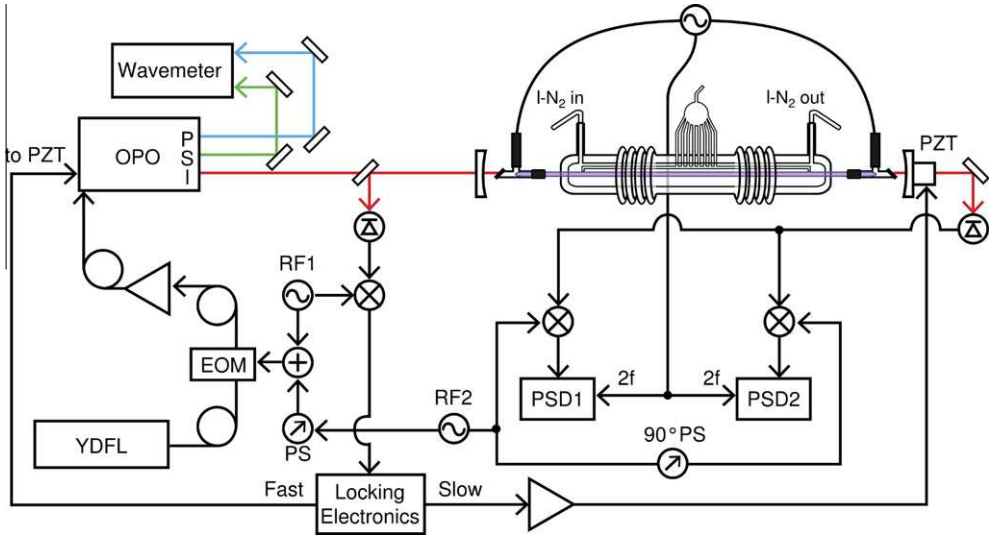

Figure 1. Block diagram of NICE-OHVMS instrument. Details of its operation are given in the main text. YDFL: Ytterbium-doped fiber laser; EOM: electro-optic modulator; OPO: optical parametric oscillator with pump (P, blue), signal (S, green) and idler (I, red) beams; PZT: piezoelectric transducer, PS: phase shifter; PSD: phase sensitive detector; •: signal splitter.

controlled with the locking electronics to maintain the resonance condition. When the cavity PZT reaches the end of its travel, the laser-cavity lock is electronically interrupted, the cavity length is reset to the other end of its travel, a new resonance is found, and the lock is reestablished. In this manner, the spectrometer can scan without manual intervention over the entire range of the YDFL PZT (around 100 GHz), although in practice a scan is generally much shorter. It is in principle possible to extend the automated tuning range further by electronic control of the intracavity etalon of the OPO and the nonlinear crystal position/temperature, but the practical utility of such efforts would likely be minimal.

3. Results and analysis

3.1. Lineshapes

The overall Doppler lineshape for NICE-OHVMS in both absorption and dispersion has odd symmetry, and qualitatively appears similar to the third derivative of a Gaussian absorption profile. A detailed analysis of the lineshape is beyond the scope of this Letter and will be the subject of a future work, but a qualitative description follows. Consider a general NICE-OHMS lineshape such as that shown in panels a and b of Figure 2 in Ref. [8]. If the signal belongs to an ion, then the AC voltage of the plasma causes velocity modulation (VM), Doppler shifting the lineshape at the plasma frequency. As a result of the bidirectional nature of light in our optical cavity, the lineshape is simultaneously Doppler shifted to the red and to the blue by the same amount at each point in time along the plasma voltage cycle. Consequently, the time-dependent signal repeats itself every plasma half-cycle, or at twice the AC plasma frequency ($2f_{vm}$). In addition to VM, an ion also experiences concentration modulation (CM) at $2f_{vm}$, and CM may be phase shifted with respect to VM. Thus, in addition to a periodic Doppler shift at $2f_{vm}$ from VM, the lineshape amplitude varies at $2f_{vm}$ from CM. The net signal observed comes in 4 channels corresponding to the even and odd second order Fourier coefficients of the absorption and dispersion profiles affected by VM and CM.

The sub-Doppler lineshape is more straightforward. As has been discussed in regard to previous NICE-OHMS setups [19,20,9], the carrier and sidebands can each act as pumps and probes for saturation spectroscopy. The Lamb dips arising from the Bennet holes burned in the population appear at half-integer multiples of the

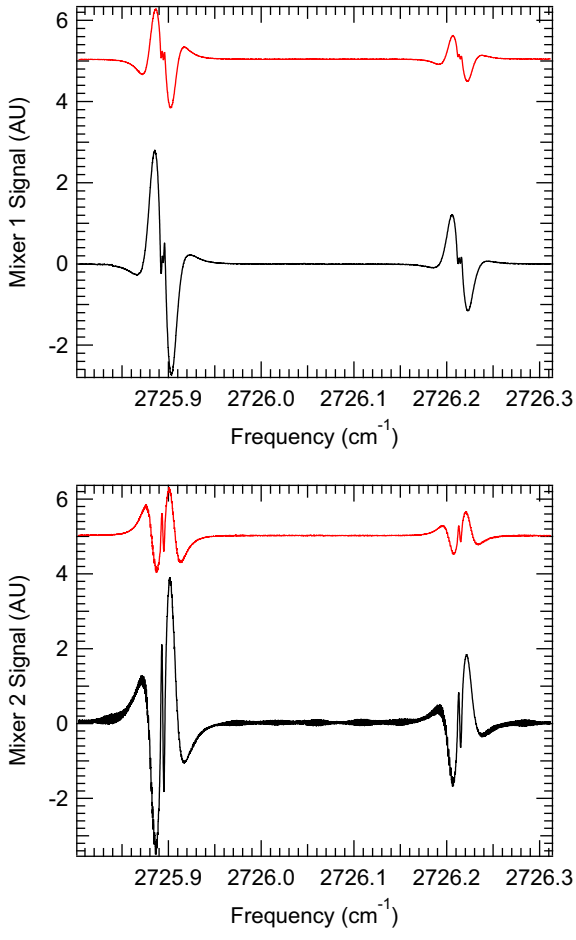

Figure 2. NICE-OHVMS spectrum of the $R(1,0)$ and $R(1,1)^u$ transitions of the ν_2 fundamental band of H_3^+. Each panel shows the in-phase (black, bottom) and quadrature (red, top) outputs of a lock-in amplifier demodulating the indicated mixer's signal.

carrier-sideband spacing f_h, i.e., at all frequencies at which forward- and reverse-propagating beams sample the same velocity component of the Doppler distribution. At the line center ν_0, when the

zero-velocity distribution is both pumped and probed by the carrier, a signal only appears in dispersion as the heterodyne detection scheme employed by NICE-OHMS is insensitive to absorption of the carrier. In the current work, the heterodyne modulation index (β) is small enough ($\sim$0.63) that only the carrier has sufficient power to saturate transitions, while the sidebands can only act as probes. The dispersion signal therefore contains Lamb dips at ν_0 and $\nu_0 \pm f_h/2$, while the absorption signal contains them at $\nu_0 \pm f_h/2$.

While VM and CM have a strong influence on the lineshape of the Doppler profile, they do not affect the sub-Doppler features in the same way. Because Bennet holes are only burned in the population at or spaced evenly around the zero-velocity component of the ion distribution, VM effectively changes the abundance of ions with the appropriate velocity. In that way, VM effectively behaves like CM, and the net effect is to influence the amplitude of the Lamb dip lineshape and the relationship between the amplitudes of the even and odd Fourier coefficients within absorption or dispersion. Neglecting any change of the ions' collision rate with changing velocity, VM and CM do not affect the sub-Doppler profile beyond its amplitude. The sub-Doppler lineshape function [9] is

$$\chi(\nu_d) = \left(A_1\left[\chi_a\left(\nu_d - \frac{f_h}{2}\right) - \chi_a\left(\nu_d + \frac{f_h}{2}\right)\right]\right)\sin\theta_h + \left(-2A_0\chi_d(\nu_d) + A_1\left[\chi_d\left(\nu_d - \frac{f_h}{2}\right) + \chi_d\left(\nu_d + \frac{f_h}{2}\right)\right]\right)\cos\theta_h, \quad (1)$$

where ν_d is the frequency detuning from the transition center frequency, θ_h is the heterodyne detection phase, A_0 is the effective amplitude of the central (carrier-carrier) dispersion Lamb dip, and A_1 is the effective amplitude of the carrier-sideband Lamb dips for absorption and dispersion. $\chi_a(\omega)$ is a Lorentzian lineshape function for absorption, and $\chi_d(\omega)$ is a lineshape function for dispersion related to $\chi_a(\omega)$ by the Kramers–Kronig relations. These are defined as

$$\chi_a(\omega) = \frac{1}{1+\gamma^2(\omega-\omega_0)^2} \text{ and } \chi_d(\omega) = \frac{-(\omega-\omega_0)\gamma}{1+\gamma^2(\omega-\omega_0)^2},$$

where ω_0 is the center and γ is the inverse of the half-width at half-maximum. When using this fit function, f_h is held at the cavity FSR (79.12 MHz), the amplitudes are constrained such that $A_0 > A_1$, and the Doppler profile near the line center is approximated by a third-order polynomial with the quadratic term set to 0.

3.2. H_3^+ Spectra

A sample spectrum of the $R(1,0)$ and $R(1,1)^u$ transitions of the ν_2 fundamental band of H_3^+ is shown in Figure 2. The signals in the top and bottom panels are the demodulated in-phase (black) and quadrature (red, offset) components of the two mixers, which in our setup we measure to be 96° out of phase with one another. The in-phase components of the $R(1,0)$ transition are shown in greater detail in Figure 3. The overall lineshape is slightly asymmetric; the blue side of the transition is stronger than the red side, particularly in mixer 2. The origin of this asymmetry is unknown, and its impact on the spectroscopic accuracy will be discussed below.

A simultaneous fit of the $R(1,0)$ sub-Doppler features in all four detection channels to Eq. (1) is shown in Figure 4. A number of constraints were employed to ensure that the fit parameters were all internally consistent. The line center frequency and Lamb dip width were forced to be equal for all four data channels. Mixers 1 and 2 were held at 96° apart, and the sideband spacing was held equal to the cavity FSR of 79.12 MHz. Because the in-phase and quadrature components of each mixer sample different blends of CM and VM, the Lamb dip amplitudes were allowed to be different for the in-phase channels and the quadrature channels. However, the two in-phase channels were forced to have equal Lamb-dip amplitudes, and likewise for the two quadrature channels. After all of these

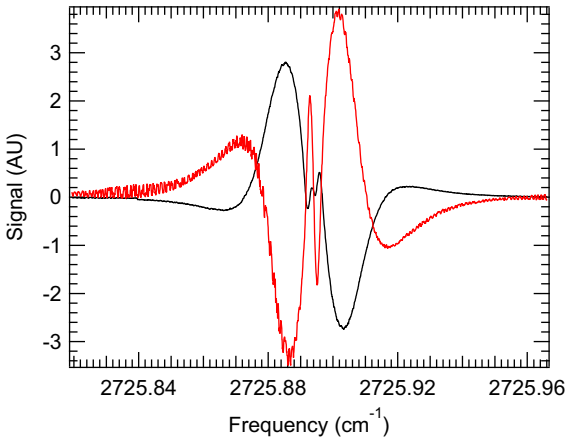

Figure 3. NICE-OHVMS spectrum of the $R(1,0)$ transition of the ν_2 fundamental band of H_3^+. The black trace is the in-phase output of mixer 1, and the red is the in-phase output of mixer 2.

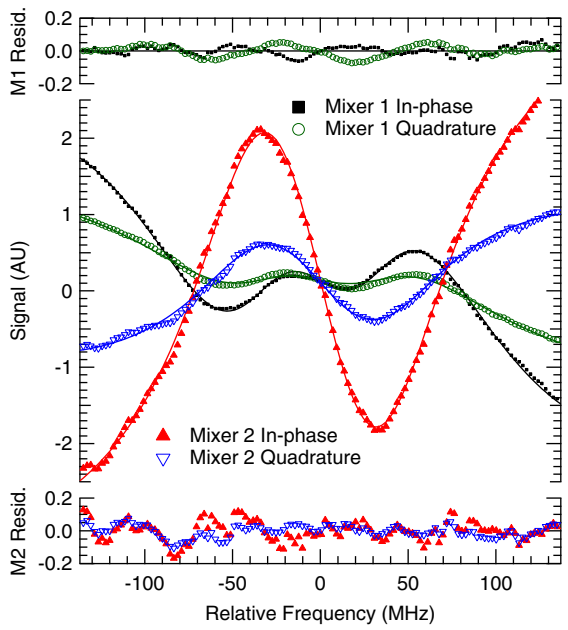

Figure 4. A simultaneous fit of the central sub-Doppler region of the H_3^+ $R(1,0)$ transition from all four data channels to Eq. (1). The symbols in the central portion of the graph are the data, and the solid lines are the fit results. The residuals of the fits are shown in the upper panel for mixer 1 and in the lower panel for mixer 2; in each case the symbols correspond to those in the central panel.

constraints, there are a total of 19 fit parameters for the entire data set: the line center frequency ν_0, the Lamb dip full width at half maximum ($2/\gamma$), the overall detection phase θ_h, Lamb dip amplitudes A_0 and A_1 for the in-phase channels and the quadrature channels, and baseline terms of the form $c_0 + c_1x + c_3x^3$ to approximate the central portion of the Doppler profile in each channel.

The overall quality of the fit is quite good; the residuals are composed primarily of fringing evident on top of the spectrum (especially mixer 2) with the notable exception of the quadrature channel of mixer 1, which has some small systematic deviations on the Lamb dips. The line center ν_0 derived from the fit is $2725.89401954 \pm 0.0000023$ cm^{-1}, but the absolute accuracy is limited by the $> 2 \times 10^{-3}$ cm^{-1} accuracy of the wavemeter, so the exact frequency should not be trusted. More important is the uncertainty of the line center determination, which is $\sim$70 kHz; this represents the maximum potential accuracy of the technique provided suitable frequency calibration is made (but see the discussion

below about the effects of the asymmetry). The overall detection phase θ_h was found to be 132°, indicating a blend of absorption and dispersion in each mixer. Because the Lamb dip widths (full width at half maximum of ~110 MHz as indicated by our fit) are much broader than the Lamb dip spacing of 39.56 MHz ($f_h/2$), the individual Lamb dips for absorption and dispersion cannot be resolved at any RF detection phase. Rather than tuning the phase to separate absorption from dispersion in the two mixers, a phase of 132° was chosen because it was found to isolate the fringing as much as possible in a single detection channel (mixer 2 in-phase), thus minimizing the fringing in the other 3 channels.

4. Discussion

The most interesting aspect of the NICE-OHVMS technique is the presence of Lamb dips which enables high precision measurements of line center frequencies. Prior to the development of NICE-OHVMS, the only methods capable of routine sub-Doppler molecular ion spectroscopy utilized fast ion beams which, due to kinematic compression, give linewidths on the order of 10 to 120 MHz [21–23]. The linewidths from ion beams are comparable to the Lamb dips presented here, though the current work with a positive column has the advantage of much higher ion density than that within an ion beam.

With the H_3^+ Lamb dip linewidths of ~110 MHz demonstrated here, the precision of the line center determination is on the order of 70 kHz. In its present implementation, the technique's accuracy is limited by the wavemeter, and also by slow drifts in the frequency of the signal and idler beams caused by thermal fluctuations of the OPO cavity. Use of an optical frequency comb to stabilize and measure the frequencies of the pump and signal beams would reduce the accuracy uncertainty to < 100 kHz. Ultimately, the total uncertainty of the technique will be determined by the reproducibility of line center determinations once appropriately calibrated.

The asymmetry observed in the overall NICE-OHVMS lineshape can adversely affect the overall accuracy. As mentioned above, the origin of this asymmetry is unknown, although it varies with heterodyne detection phase; similar effects were not observed in the near-IR implementation of NICE-OHVMS [9]. Nevertheless, we have performed simulations of the effects of the asymmetry by synthesizing skewed profiles and comparing the results of our fit function to the actual location of the Lamb dips. Based on the fitting of our simulations, we estimate the magnitude of this line center shifting to be less than a few MHz, even for Doppler profiles that are much more asymmetric than those shown in this Letter. Further study of this phenomenon will be possible with an optical frequency comb, and such work is envisioned in the near future.

The width of the Lamb dips (~110 MHz FWHM from the fitting) is fairly broad. We have varied the intracavity laser power and the cell pressure, but any differences in the linewidth were not observable. However, the ranges of the power and pressure measurements were limited: the intracavity power could only be changed by a factor of 2 before the laser-cavity lock was adversely affected, and the plasma could only give stable operation over 200–600 mTorr. Such wide Lamb dips were also observed in the NICE-OHVMS experiment performed on N_2^+ in the near-IR [9]; in that study, the authors were able to observe a change in linewidth with pressure, but extrapolating to zero pressure still gave a linewidth of ~30 MHz. Assuming that the linewidth is related to the time an ion spends at zero velocity, it is perhaps unsurprising that a less massive ion like H_3^+ has a broader linewidth than N_2^+, as its velocity may be more easily altered by weak long-range interactions.

The fringing apparent in the figures above limits the sensitivity of the present measurements in 2 of the 4 detection channels. The origin of the fringing is not fully understood; however, it appears to have a definite phase with respect to both the heterodyne detection and the plasma modulation. When the plasma is turned off, the fringing does not appear in a scan, and if the cavity transmission detector is blocked while a signal originating from a single fringe is present on a lock-in channel, the signal vanishes. Thus, it appears that the fringing is the result of the plasma interacting with the laser light rather than a purely electronic effect. One possibility is that residual amplitude modulation (RAM) in the heterodyne sidebands is being modulated by the plasma. RAM is an imbalance in the amplitude and/or phase of the sidebands with respect to one another. When demodulated, RAM appears as a DC offset in the heterodyne signal; because of our detection scheme using velocity modulation and $2f$ detection, the NICE-OHVMS would ordinarily be insensitive to such an offset. However, if the refractive index of the plasma varies at $2f$, the DC signal from RAM will be modulated at $2f$ as well, resulting in a net NICE-OHVMS signal. Because RAM is also affected by the presence of etalons in the optical system and the optical frequency, a fringing pattern could possibly result as a function of laser frequency. Testing whether this is truly the origin of the fringing is difficult; however, it is probable that the fringing would be reduced by employing a RAM compensation scheme via temperature and voltage control of the fiber EOM [24].

The sensitivity of the technique at the experimental detection bandwidth of 16 Hz, as determined from the noise-equivalent absorption in the baseline of the in-phase component of mixer 1 (which has the least fringing of the four detection channels), is 3.4×10^{-9} cm^{-1}. which is about two orders of magnitude above the shot noise limit of 3.9×10^{-11} cm^{-1} calculated from

$$\alpha_{\min} = \frac{\pi}{2F}\sqrt{\frac{eB}{\eta P_0}}\frac{1}{J_0(\beta)J_1(\beta)L}, \tag{2}$$

where F is the cavity finesse (120), e the fundamental electric charge, B the detection bandwidth (16 Hz), η the detector responsivity, P_0 the power incident on the detector, $J_n(\beta)$ the nth order Bessel function for modulation index β (0.63), and L the cavity length (190 cm). While NICE-OHMS has been able to achieve a noise level within a factor of 2 of the shot noise limit in one implementation [7], the performance achieved by NICE-OHVMS relative to the shot noise limit is already comparable to a number of other NICE-OHMS setups (see the extensive discussion in Section 4 of [8]).

Ultimately, the absolute sensitivity can be improved by identifying and eliminating noise sources and by increasing the cavity finesse. An increase in cavity finesse leads to additional technical challenge in maintaining the laser-cavity lock, and may make the system even more susceptible to the fringing effects that have already been observed. Such challenges can likely be overcome by improving the bandwidth of the laser frequency corrections (currently limited to the 10 kHz bandwidth of the signal cavity PZT), and correcting for RAM as discussed above.

5. Conclusions

In this Letter, we have demonstrated sub-Doppler spectroscopy of molecular ions in the mid-infrared spectral region using the NICE-OHVMS technique with a cw-OPO. By phase modulating the seed laser with a fiber EOM prior to amplification and optical parametric oscillation, the mid-infrared idler is also phase modulated without requiring a mid-IR EOM. The high optical power of the idler beam allows use of high-bandwidth detectors, which in turn make ultra-sensitive spectroscopy via NICE-OHMS possible. Velocity modulation spectroscopy is then combined with NICE-OHMS to afford ion-neutral discrimination, and the intracavity laser power is sufficient for saturating fundamental rovibrational transitions as demonstrated by spectroscopy of H_3^+. By fitting the sub-Doppler spectral features, the center frequencies of individual rovibrational lines can be measured with a precision of 70 kHz, and the maximum

achieved sensitivity is within a factor of ~90 of the shot noise limit. Improvements to the technique, such as addition of an optical frequency comb for accurate wavelength calibration, technical modifications to improve its sensitivity, and expanding the frequency coverage of the OPO from 3.2–3.9 μm to 2.8–4.8 μm, are envisioned.

The authors thank Takeshi Oka for providing us with the liquid nitrogen cooled plasma cell and its associated pumps and plasma electronics. KNC and BMS acknowledge support from a NASA Earth and Space Science Fellowship. JNH acknowledges support from a Springborn Fellowship and a National Science Foundation Graduate Research Fellowship (DGE 11-44245 FLLW). This work has been supported by the National Science Foundation (PHY 08-55633), the NASA Laboratory Astrophysics program (NNX08AN82G), and a David and Lucile Packard Fellowship.

References

[1] C.S. Gudeman, M.H. Begemann, J. Pfaff, R.J. Saykally, Phys. Rev. Lett. 50 (1983) 727.
[2] C.S. Gudeman, M.H. Begemann, J. Pfaff, R.J. Saykally, J. Chem. Phys. 78 (1983) 5837.
[3] S.K. Stephenson, R.J. Saykally, Chem. Rev. 105 (2005) 3220.
[4] B.M. Siller, A.A. Mills, B.J. McCall, Opt. Lett. 35 (2010) 1266.
[5] A.A. Mills, B.M. Siller, B.J. McCall, Chem. Phys. Lett. 501 (2010) 1.
[6] L.C. Sinclair, K.C. Cossel, T. Coffey, J. Ye, E.A. Cornell, Phys. Rev. Lett. 107 (2011) 093002.
[7] J. Ye, L.-S. Ma, J.L. Hall, J. Opt. Soc. Am. B 15 (1998) 6.
[8] A. Foltynowicz, F. Schmidt, W. Ma, O. Axner, Appl. Phys. B 92 (2008) 313.
[9] B.M. Siller, M.W. Porambo, A.A. Mills, B.J. McCall, Opt. Exp. 19 (2011) 24822.
[10] M.S. Taubman, T.L. Myers, B.D. Cannon, R.M. Williams, Spectrochim. Acta 60 (2004) 3457.
[11] M.W. Porambo, B.M. Siller, J.M. Pearson, B.J. McCall, Opt. Lett., in press.
[12] W.D. Watson, Astrophys. J. 183 (1973) L17.
[13] E. Herbst, W. Klemperer, Astrophys. J. 185 (1973) 505.
[14] T. Oka, Phys. Rev. Lett. 45 (1980) 531.
[15] C.M. Lindsay, B.J. McCall, J. Mol. Spectrosc. 210 (2001) 60.
[16] C.P. Morong, J.L. Gottfried, T. Oka, J. Mol. Spectrosc. 255 (2009) 13.
[17] L. Velilla, B. Lepetit, A. Aguado, J.A. Beswick, M. Paniagua, J. Chem. Phys. 129 (2008) 084307.
[18] C. Lindsay, E.T. White, T. Oka, Chem. Phys. Lett. 328 (2000) 129.
[19] A. Foltynowicz, W. Ma, O. Axner, Opt. Exp. 16 (2008) 14689.
[20] O. Axner, W. Ma, A. Foltynowicz, J. Opt. Soc. Am. B 25 (2008) 1166.
[21] C.S. Gudeman, R.J. Saykally, Ann. Rev. Phys. Chem. 35 (1984) 387.
[22] J.V. Coe, J.C. Owrutsky, E.R. Keim, N.V. Agman, D.C. Hovde, R.J. Saykally, J. Chem. Phys. 90 (1989) 3893.
[23] A.A. Mills, B.M. Siller, M.W. Porambo, M. Perera, H. Kreckel, B.J. McCall, J. Chem. Phys. 135 (2011) 224201.
[24] I. Silander, P. Ehlers, J. Wang, O. Axner, J. Opt. Soc. Am. B 29 (2012) 916

Kyle Crabtree graduated with a B.S. in Chemistry from Ball State University in 2006, and received his Ph.D. in Chemistry from the University of Illinois in 2012. He is currently a CfA Postdoctoral Fellow at the Harvard-Smithsonian Center for Astrophysics.

James Hodges received a B.S. in Chemistry and a B.S. in Polymer & Fiber Chemistry in 2010 from Clemson University. He currently attends the University of Illinois pursuing a PhD in Chemistry as a Springborn Fellow and an NSF Graduate Research Fellow.

Brian Siller graduated with a B.A. in Chemistry, Computer Science, and Mathematics from Ohio Wesleyan University in 2007, and is currently pursuing a Ph.D. in Physical Chemistry at the University of Illinois.

Adam Perry graduated with a B.S. in Chemistry from Oregon State University in 2011, and is currently a graduate student in Physical Chemistry at the University of Illinois.

Joe Kelly graduated with a B.S. in Chemistry from the University of Illinois in 2012.

Paul Jenkins II is currently pursuing his B.S. in Chemical Engineering at the University of Illinois, and plans to graduate in 2015.

Ben McCall received his Ph.D. from the University of Chicago in Chemistry and Astronomy & Astrophysics. Following a Miller Research Fellowship at the University of California at Berkeley, he joined the faculty of the University of Illinois, where he is currently an Associate Professor of Chemistry and Astronomy.

Indirect Rotational Spectroscopy of HCO^+

Brian M. Siller,[†] James N. Hodges,[†] Adam J. Perry,[†] and Benjamin J. McCall[*,†,‡]

Department of Chemistry, University of Illinois at Urbana-Champaign, and Departments of Physics and Astronomy, University of Illinois at Urbana-Champaign

E-mail: bjmccall@illinois.edu

Abstract

Spectroscopy of the ν_1 band of the astrophysically relevant ion HCO^+ is performed with an optical parametric oscillator calibrated with an optical frequency comb. The sub-MHz accuracy of this technique was confirmed by performing a combination differences analysis with the acquired rovibrational data and comparing the results to known ground-state rotational transitions. A similar combination differences analysis was performed from the same data set to calculate the previously unobserved rotational spectrum of the ν_1 vibrationally excited state with precision sufficient for astronomical detection. Initial results of cavity-enhanced sub-Doppler spectroscopy are also presented, and hold promise for further improving the accuracy and precision in the near future.

Introduction

Molecular ions are a particularly challenging group of species to study with optical spectroscopy. Even in laboratory plasmas that are designed to observe only a specific ion, neutral molecules are still orders of magnitude more abundant than their charged counterparts. This is why the most

[*]To whom correspondence should be addressed
[†]Department of Chemistry, University of Illinois at Urbana-Champaign
[‡]Departments of Physics and Astronomy, University of Illinois at Urbana-Champaign

productive techniques for ion spectroscopy tend to have some method for discriminating ionic absorption signals from neutral ones. Since the late 1980s, the predominant tool for this has been velocity modulation spectroscopy (VMS). The groundwork of VMS was laid by Wing *et al.* in a velocity modulated ion beam,[1] and the first application of VMS as it is known today was by Gudeman *et al.* in a velocity modulated positive column discharge cell.[2] Since the initial work, the technique has become a mainstay in ion spectroscopy and has been extensively reviewed.[3,4]

Protonated carbon monoxide, HCO^+, was the first ion whose spectrum was acquired using VMS. The R-branch of the ν_1 C-H stretch band was first measured by Gudeman *et al.* in a positive column discharge cell out to R(18).[2] Shortly after, the P-branch was also observed out to P(10) in a modulated DC glow.[5] After these lines were published it was another 24 years before any work revisited the ν_1 band, when Verbraak *et al.* used a continuous wave optical parametric oscillator (cw-OPO) operating in the mid-infrared and a supersonic expansion discharge source to rotationally cool the ions.[6]

The first observation of an HCO^+ rotational transition was via telescope rather than in a laboratory in 1970 by Buhl and Snyder.[7] Because the line that they observed was unidentified at the time, it was referred to as "X-ogen". Later that year, Klemperer suggested that the "X-ogen" line was due to the J = 1←0 transition of HCO^+.[8] Five years later, Woods *et al.* confirmed its identity by microwave spectroscopy.[9] Since that time, HCO^+ has been found in a variety of astronomical environments including protoplanetary nebulae,[10] star forming regions,[11] the interstellar medium,[12] and even the comet Hale-Bopp.[13] The abundance of HCO^+ makes it an important participant in the rich chemistry that exists in the interstellar medium. Due to the large rotational constant of HCO^+, its higher rotational transitions exist in the sub-millimeter/terahertz region. Newer telescopes such as The Atacama Large Millimeter and sub-millimeter Array (ALMA) and the Stratospheric Observatory For Infrared Astronomy (SOFIA) have sub-millimeter/terahertz capability. These new astronomical capabilities lend necessity to a relatively simple way to gain laboratory information in that spectral region, a challenging region for laboratory spectroscopy, due in part to the relative scarcity of quality sources and detectors compared to the microwave and infrared spectral regions.

In this work, we present a demonstration of how precision rovibrational spectroscopy can be used to infer rotational transitions to precision sufficient to facilitate astronomical searches.

In the case of HCO^+, most of the ground state transitions have been observed up to J = 17←16, with the exception of a few gaps in coverage.[14] Additionally, only a few pure rotational lines have been observed in vibrationally excited states. One such transition is the J = 3←2 rotational transition in the ν_1 first vibrationally excited state.[15] With this single transition combined with our high-precision IR spectrum, the entire rotational spectrum of the ν_1 state can be calculated, limited only by the number of rovibrational lines that have been observed. The technique demonstrated here is also useful for determining high precision rotational constants in excited states.

In this work, we present spectra of the ν_1 fundamental band of HCO^+ acquired using optical heterodyne spectroscopy coupled with VMS (OH-VMS). This technique combines the advantages of the low noise of heterodyne spectroscopy with ion-neutral discrimination of VMS. Our instrument utilizes a cw-OPO tunable from 3.2 to 3.9 μm, and produces ions within a liquid nitrogen cooled positive column discharge cell. Optical frequency comb calibrated scans were acquired and fit with sub-MHz precision, and the resulting fits were used to calculate rotational transitions for the ground state and the first vibrationally excited C-H stretch state. These calculations result in the first experimental observation, albeit indirectly, of the J = 3←2 transition in the ground state and the complete determination of the of the rotational spectrum up to J = 10←9 in the ν_1 first excited state.

Experimental

The experimental setup, shown in Figure 1, has been described previously[16] with the exception of the frequency comb integration, so it will be discussed only briefly here. A Ytterbium-doped fiber laser is frequency modulated with a fiber-coupled electro optic modulator (EOM) using two RF generators: one at ∼80 MHz for heterodyne detection, and the other at ∼2 MHz for locking to the optical cavity around the discharge cell. After the modulation is applied, this seed laser is

amplified to 10 W total power using a fiber amplifier, and this amplified beam acts as the pump for the optical parametric oscillator (OPO).

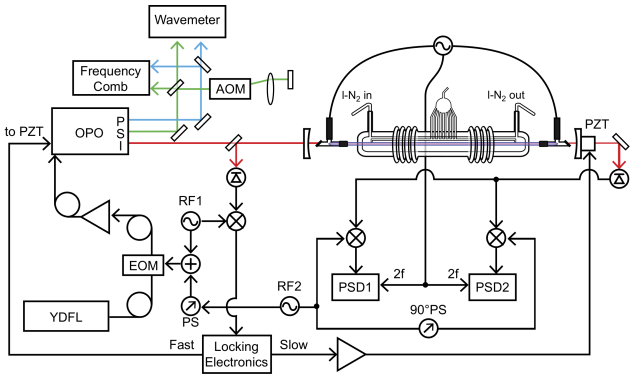

Figure 1: The Experimental Layout. YDFL: Ytterbium-doped fiber laser; EOM: electro-optic modulator; PS: phase shifter; RF: radio frequency generator; OPO: optical parametric oscillator; P,S,I: pump, signal, idler; PZT: piezo-electric transducer; PSD: phase-sensitive detector

Three beams exit the OPO head: the pump ($\sim$1064 nm), the signal (tunable from 1.5 to 1.6 μm), and the idler (tunable from 3.2 to 3.9 μm). The idler is used for spectroscopy of HCO^+ while the other beams are used for frequency measurements using a near-infrared wavemeter and frequency comb. For the comb-calibrated scans, the wavemeter is only used prior to a scan to determine which comb modes the pump and signal are each closest to, while the comb is used throughout the scan to take frequency readings at each acquired data point.

Comb Integration

The optical frequency comb used in this work (Menlo FC1500) has been described previously in operation with a different laser system.[17] Scanning the OPO with the comb is accomplished by first tuning the carrier-envelope offset of the comb to approximately 20 MHz and determining its sign. Then the comb repetition rate is tuned to make the signal offset beat lie within the range of 25-35 MHz from the nearest comb mode, limited by the RF bandpass filter built into the frequency counter used to record that beat. Then the frequency of the pump is tuned to approximately 20 MHz from its nearest comb mode, and the signs of the offset beats for both the pump and the signal are determined and recorded. Finally, the pump is offset-locked to the comb using a frequency-to-

voltage converter circuit that generates an appropriate error signal for offset locking.

The nearest comb mode numbers are determined for the pump and the signal before each scan using the wavemeter, then are recorded (and incremented/decremented for the signal when necessary) as the scan progresses. At each frequency step, the data acquisition program pauses for 1.5 seconds, then the comb repetition rate and offset beats are recorded by frequency counters with 1 Hz refresh rates, and the lock-in amplifier outputs are recorded. With the lock-in amplifier time constant set to 300 ms, the lock-in amplifiers have 5 time constants to respond before the reading is polled for each point, so any scanning direction dependent line center pulling is smaller than the random scan-to-scan variability in line center determination.

After each point, the repetition rate is tuned by an amount sufficient to slew the pump frequency by $\sim$5 MHz ($\sim$1.8 Hz change in repetition rate). The pump remains offset locked to the same comb mode throughout the course of each scan. The total continuous scanning range of the pump (and therefore for the idler) for comb-calibrated scans is limited to $\sim$800 MHz by the comb scanning electronics; the comb repetition rate can only be changed by a relatively small amount while still retaining its lock onto the direct digital synthesizer (DDS) that stabilizes the repetition rate.

To keep the signal offset within the frequency counter bandpass filter at each point, a feed-forward system is used to tune the signal frequency using a double-pass acousto-optic modulator (AOM) setup. In a double-pass configuration, the frequency shift induced by the AOM is doubled, while making the pointing of the beam independent of the frequency applied to the AOM.[18] Stable pointing is crucial to the operation of the system, as good spatial overlap between the comb light and each of the cw beams is important for generating offset beat signals on the high speed detectors.

After the counters are read for a data point and the repetition rate is slewed to the next point, the amount the signal frequency needs to be shifted by is calculated using the change in the repetition rate, the signal comb mode number, and the amount the signal was away from the 30 MHz target offset frequency for the previous point; this frequency shift is then applied to the frequency of the RF generator that drives the AOM. The AOM diffraction efficiency is high enough to provide reliable signal/comb offset beat measurements in the driving frequency range of 150-210 MHz,

which corresponds to a frequency shift of 300-420 MHz when taking into account the double-pass configuration. When the calculated desired AOM frequency lies outside this range, the drive frequency is shifted by 50 MHz (corresponding to a 100 MHz change in the shifted signal frequency, matching the comb repetition rate), and the signal mode number is incremented or decremented by one, depending on whether the 100 MHz shift was positive or negative.

This signal-shifting scheme allows the shifted signal frequency to be determined using the frequency comb at each point, despite the fact the signal frequency is fixed (with the exception of some slow drift) while the comb repetition rate is slewing. The unshifted signal frequency can then be determined simply by subtracting the AOM frequency shift, which is precisely known from the digital setting of the RF generator at each point, and this unshifted signal frequency is subtracted from the directly measured pump frequency to determine the idler frequency.

Spectroscopy Configuration

The plasma cell used in this work, Black Widow, shown in Figure 2, was the same cell used by Takeshi Oka in many of his velocity modulation experiments. It allows for liquid nitrogen cooling of the plasma to reach an estimated rotational temperature of $\sim$166 K for HCO^+, as shown in the Boltzmann plot in Figure 3, using plasma conditions of 30 mTorr CO in 500 mTorr H_2 with a 35 kHz, 140 mA discharge. The idler beam is coupled through Brewster windows on either end of the cell into the central bore of the discharge cell. For this work, three different optical configurations were used: single-pass, double-pass and cavity-enhanced, all of which relied on heterodyne modulation and detection at $\sim$80 MHz.

The comb calibrated scans presented in this paper used a simple single-pass configuration, where the cavity mirrors shown in Figure 1 were removed and the cavity-locking RF modulation and feedback circuit were disabled. This allowed for the acquisition of Doppler-broadened scans with signal-to-noise ratios of $\sim$300 for the strongest lines and $\sim$100 for the weakest ones, but due to the lack of a bidirectional beam and sufficient laser power, did not allow for the observation of Lamb dips. A typical comb-calibrated scan is shown in Figure 4.

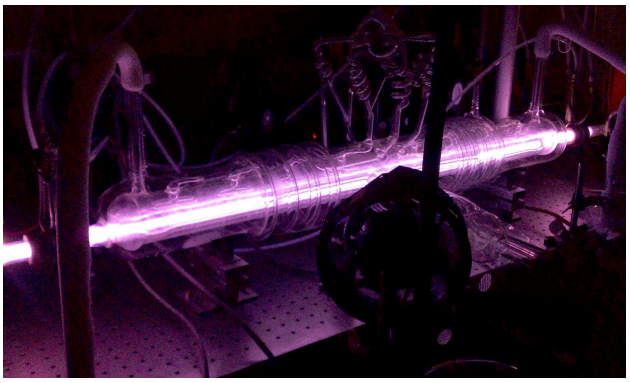

Figure 2: "Black Widow", the liquid nitrogen cooled positive column discharge cell acquired from Takeshi Oka and used for the work in this paper. The central bore, where the plasma discharge occurs, is surrounded by a sheath of flowing liquid nitrogen, which is in turn surrounded by a vacuum jacket to prevent ice from forming on the cell.

A series of double-pass wavemeter-calibrated scans were collected for the previously unobserved P(11) through P(17) transitions. In the double-pass configuration, a single mirror was placed on the far side of the cell to back-reflect the idler for a second pass through the cell. Approximately 30% of the reflected beam was then picked off with a silicon window and directed to a high-speed detector, the signal from which was demodulated first at the heterodyne frequency, then at twice the plasma frequency ($2f$), as opposed to the $1f$ demodulation that was used for the single-pass work. The linecenters determined from these scans are shown in Table 1, and compared to the calculated values from the fit parameters determined by the comb-calibrated work. All but one of the linecenters determined from these scans fall within the expected 70 MHz uncertainty from the wavemeter calibration. The one exception, P(17), is thought to be off by more than the uncertainty due to an inaccurate signal reading caused by poor optical alignment.

A few uncalibrated scans were collected with the cavity mirrors in place in a noise immune cavity enhanced optical heterodyne velocity modulation spectroscopy (NICE-OHVMS)[19] configuration. One such scan, showing strong central Lamb dip features on top of the Doppler profile, is shown in Figure 5. Unfortunately, the dielectric coatings on the mirrors were found to be hygroscopic, which led to poor laser coupling efficiency through the cavity in this wavelength range and degraded performance over time. To obtain optimal Lamb dip depth, the total cell pressure had to be decreased to $\sim$200 mTorr and the discharge current had to be turned down as low as

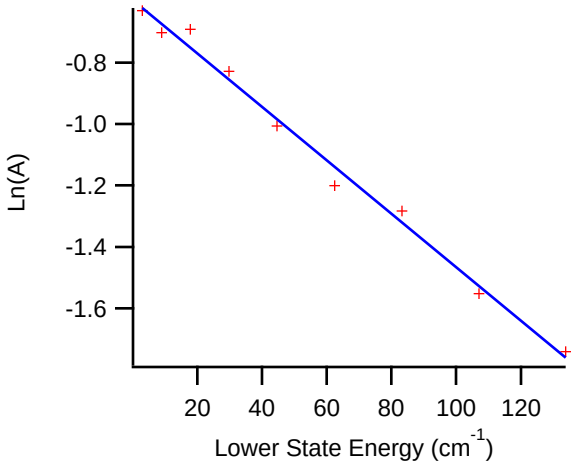

Figure 3: Boltzmann plot for R(1) through R(9), with the slope indicating a plasma temperature of ∼166 K. The vertical axis is the natural log of the line strength normalized peak-to-peak amplitude of a double-pass scan for each transition.

Table 1: Previously unobserved wavemeter-calibrated scans of the P(11) through P(17) transitions. Uncertainties are ∼70 MHz, limited by the wavemeter uncertainties for the pump and signal frequencies added in quadrature. Calculations are based on ground state constants from Cazzoli *et al.* [14] and excited state constants determined from our comb-calibrated scans.

Transition	Observed (cm^{-1})	Calculated (cm^{-1})	Obs - Calc (MHz)
P(11)	3054.730	3054.73019(4)	-6
P(12)	3051.502	3051.49993(5)	62
P(13)	3048.245	3048.24688(6)	-57
P(14)	3044.969	3044.97111(7)	-63
P(15)	3041.672	3041.67269(8)	-21
P(16)	3038.354	3038.35169(9)	69
P(17)	3035.013	3035.00817(10)	145

possible while still maintaining a stable plasma, to ∼100 mA. Both the lower pressure and the lower discharge current produce lower overall density of HCO^+ within the cell. This decreased density combined with the poor laser transmission through the cavity cause the signal-to-noise in the NICE-OHMS scans to be significantly compromised compared to the single- and double-pass scans, despite the factor of ∼400 greater path length that NICE-OHMS provides through the plasma.

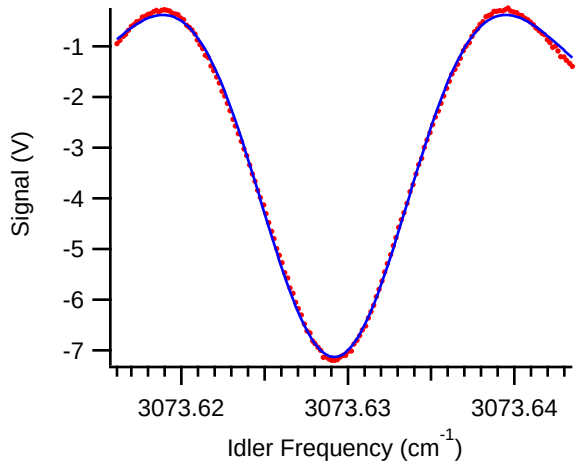

Figure 4: A typical comb-calibrated scan (red dots) of the P(5) transition of HCO^+, along with a fit to the data (blue line). Error bars for the points are not shown, as they would be smaller than the point size for both intensity and frequency.

Results and Discussion

Each comb calibrated scan was fit to a second derivative of a Gaussian function, which approximates the convolution of heterodyne modulation with velocity modulation observed in the experiment. Between 4 and 7 scans were acquired of each transition, and the data acquired from those fits were used to compute the average linecenters and standard errors shown in Table 2. The errors varied somewhat from one transition to the next, but the average uncertainty was found to be $\sim$600 kHz.

As can be seen by the fit in Figure 4, this fit function is not perfect, likely due to imperfect setting of the detection phases. For this work, both the RF and plasma demodulation phases were set to maximize the signal-to-noise of a single detection channel out of the four channels that were acquired with each scan. It is likely that there is some dispersive component to the lineshape function, rather than it being purely absorptive. It is also likely that the velocity modulation of the ions is not purely sinusoidal and that the lock-in demodulation is not exactly in phase with the velocity modulation, and both of these factors can also affect the overall lineshape.

There is also a slight asymmetry in the observed lineshapes for several of the scans that is not fully understood at this time. By adding a slightly sloped baseline to the data, we can make it

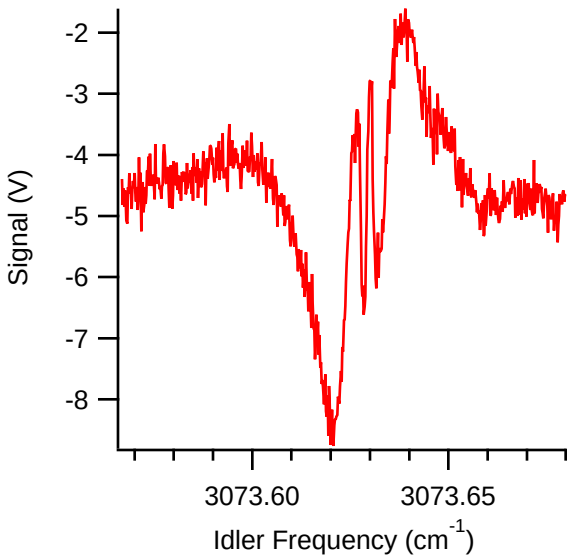

Figure 5: A roughly calibrated scan of the P(5) transition of HCO^+, showing the Lamb dips that are obtainable with cavity enhancement combined with lower cell pressure. The frequency calibration of this scan was based on the line center determined from the comb calibrated scans combined with the approximate scan voltage to frequency transfer function of the seed laser.

significantly more symmetric, and also make the fit slightly better. Symmetrizing the data in this way causes the determined linecenter to shift by less than 1 MHz for even the most asymmetric scans. Given that we do not know the physical cause of this phenomenon, we have taken the approach of manipulating the data as little as possible, so this symmetrizing was only done to estimate the potential error induced by the asymmetry. When asymmetry is present, it tends to manifest with the low-frequency lobe of the lineshape having a greater maximum than the high-frequency one. Such a systematic error would be mitigated by subtraction of observed linecenters, as is done in the combination differences analysis described in the following several paragraphs. Based on the errors in the calculation of rotational transitions, it appears that random scan-to-scan variability is the limiting factor in linecenter determination, and not the effects of this asymmetry.

For approximately half of the comb-calibrated scans, the determined linecenters disagreed with the previously measured HCO^+ transition frequencies[5] by greater than the specified accuracy of 30 MHz. It was found that the source of the errors was incorrect comb mode number determination for either the signal or the pump beams due to inaccuracy of the wavemeter. These incorrectly

Table 2: A list of the comb-calibrated HCO^+ transition center frequencies (with associated uncertainties) observed in the current work, compared with previous measurements.

Transition	Linecenter (cm^{-1})	Previous Work[5] (cm^{-1})	Previous-Current (MHz)
R(0)	3091.690432(16)	3091.6919(10)	44
R(1)	3094.618099(27)	3094.6181(10)	0
R(2)	3097.522054(07)	3097.5223(10)	7
R(3)	3100.402249(25)	3100.4034(10)	35
R(4)	3103.258604(21)	3103.2586(10)	0
R(5)	3106.090956(19)	3106.0909(10)	-2
R(6)	3108.899376(20)	3108.9002(10)	25
R(7)	3111.683680(04)	3111.6841(10)	13
R(8)	3114.443835(05)	3114.4445(10)	20
R(9)	3117.179881(41)	3117.1800(10)	4
P(1)	3085.763903(23)	3085.7646(10)	21
P(2)	3082.765487(53)	3082.7662(10)	21
P(3)	3079.743422(15)	3079.7437(10)	8
P(4)	3076.698005(05)	3076.6977(10)	-9
P(5)	3073.629188(16)	3073.6291(10)	-3
P(6)	3070.537136(19)	3070.5377(10)	17
P(7)	3067.421924(37)	3067.4224(10)	14
P(8)	3064.283464(10)	3064.2834(10)	-2
P(9)	3061.122045(18)	3061.1226(10)	17
P(10)	3057.937606(08)	3057.9380(10)	12

calibrated scans were easily corrected by adding or subtracting a multiple of the comb repetition rate to or from the calculated idler frequency. After correcting the idler frequency calibration, it was found that all but two of the the observed transitions agreed with Amano's previous work to within 30 MHz. The two exceptions to the 30 MHz agreement were the R(0) and R(3) transitions, but those were both further verified by comparing the combination difference analysis with directly measured rotation transitions, as shown in Table 3. Any remaining error in the determination of comb mode numbers would appear as an error of $\sim$100 MHz, which is not observed.

A combination differences analysis was performed to demonstrate the accuracy of our comb-calibrated rovibrational compared to known rotational transitions. First, frequencies of transitions sharing the same upper state energy level, e.g. R(0) and P(2), were subtracted from one another to generate ground state energy level spacings for pairs of energy levels separated by two rotational energy levels. For example, the J=2$\leftarrow$0 spacing was calculated from $f_{R(0)} - f_{P(2)}$, the J=3$\leftarrow$1

Table 3: Indirectly calculated rotational transition frequencies derived from the data in Table 2 compared to the directly measured rotational transitions compiled by Cazzoli *et al.*[14]

J'	J"	Calc. Freq. (MHz)	Obs. Freq.[14] (MHz)	Calc - Obs (MHz)
0	1	n/a	89188.5247	n/a
1	2	178374.6(17)	178375.0563	-0.5
2	3	267557.0(19)	n/a	n/a
3	4	356732.3(19)	356734.2230	-2.0
4	5	445903.9(21)	445902.8721	1.0
5	6	535061.0(23)	535061.5810	-0.5
6	7	624207.4(26)	624208.3606	-1.0
7	8	713344.0(27)	713341.2278	2.8
8	9	802455.7(27)	802458.1995	-2.5
9	10	891558.4(27)	891557.2903	1.1

spacing was calculated from $f_{R(1)} - f_{P(3)}$, and so forth for all observed transitions up to the J=10←8 spacing.

Then the directly measured J=1←0 transition was subtracted from the J=2←0 energy level spacing to indirectly compute the J=2←1 rotational transition frequency. This computed frequency was then subtracted from the J=3←1 spacing to compute the J=3←2 transition frequency, and the process was repeated for higher rotational energy levels up to J=10←9. At each step, the calculated rotational transition from the previous step was used with a new energy level difference to compute a new rotational transition. The indirectly calculated rotational transitions in the current work are compared to the previously observed rotational transition frequencies in Table 3.

Such an analysis was also carried out for the ν_1 (C-H stretch mode) first vibrationally excited state. To our knowledge, the only directly observed rotational transition was J=3←2.[15] This single transition, combined with our rovibrational data, is sufficient to compute the expected rotational transitions from J=1←0 up to J=10←9, as shown in Table 4. The comb-calibrated data were also fit using the previously determined ground state constants,[14] and the following vibrationally excited state constants were determined: ν_1 = 3088.739009(5) cm^{-1}, B_1 = 44240.536(9) MHz, and D_1 = 82.31(9) kHz. These values agree within 2σ with the uncertainties those previously determined by Amano [3088.73951(31) cm^{-1}, 44240.34(33) MHz, and 80.3(33) kHz] using infrared spectroscopy,[5] while disagreeing by 5σ with the B_1 and D_1 determined by an "all-inclusive" fit by

Lattanzi *et al.* that used data from several microwave and infrared papers to determine constants across several vibrational states to determine B_1 = 44240.614(17) MHz and D_1 = 86.56(82) kHz.[15] Given that the only data for the ν_1 state included in the "all-inclusive" fit were Amano's infrared spectrum (which reported transitions with 30 MHz uncertainties) and a single rotational transition (J=3←2),[20] we do not currently understand the small magnitude of uncertainties reported by Lattanzi *et al.*

Table 4: Pure rotational transitions for the vibrationally excited ν_1 state of HCO^+, calculated from the rovibrational data in Table 2 and the directly observed[15] J=3←2 rotational transition.

J'	J"	Calc. Freq. (MHz)	Uncertainty (MHz)
0	1	88486.7	1.9
1	2	176955.4	1.6
2	3	n/a	n/a
3	4	353900.7	0.9
4	5	442366.0	1.1
5	6	530813.3	1.3
6	7	619257.7	1.6
7	8	707676.3	1.9
8	9	796093.7	1.9
9	10	884477.9	2.4

Conclusions

The current work demonstrates the ability of Doppler-broadened comb-calibrated velocity modulation spectroscopy to determine linecenters with sub-MHz accuracy and precision. This accuracy has been verified by performing a combination differences analysis of the rovibrational data and comparing the results to the previously observed rotational spectrum of vibrational ground state HCO^+. The potential of extending the technique to sub-Doppler work has also been demonstrated. With a proper set of cavity mirrors, it should be possible to further improve the precision of this technique. From the current series of fits, the Doppler-limited linewidth is ∼450 MHz, and the uncertainty of a single fit is ∼350 kHz. From the Lamb dip scan of HCO^+ shown in Figure 5, the peak-to-peak linewidth of the central sub-Doppler feature is only ∼50 MHz, so it is reasonable

to assume that the precision of a fit to sub-Doppler features would be approximately an order of magnitude more precise than one to a Doppler-broadened scan, assuming the S/N problem can be solved by a non-hygroscopic set of cavity mirrors. The investigation into whether the accuracy is also improved by the same factor will be the subject of future work.

One of the greatest advantages of this indirect approach over direct rotational spectroscopy is the generality of it. The chemistry within positive column discharge cells tends to be very rich, so it is possible to make a wide variety of molecular ions. The cell used in the current work was cooled with liquid nitrogen, but it could easily be cooled by water or air, or even heated to attain greater population in higher rotational levels and compute the rotational spectrum up to very high J values. The infrared source and detectors are also very versatile in terms of spectral coverage; entire rovibrational bands for a wide variety of ions lie within its tuning range, and can be observed without any changes to the optoelectronic system.

This work also has implications for astronomical searches for the astrophysically relevant ion HCO^+. While the ground vibrational state has been thoroughly studied, little work has previously been done in this vibrationally excited state. Rotational transitions in the vibrationally excited state could be of astrophysical interest, particularly in hot, dense environments such as hot cores and circumstellar envelopes.[21]

Acknowledgments

The authors would like to acknowledge an NSF grant (CHE 12-13811) and a NASA Laboratory Astrophysics grant for funding. BJM wishes to acknowledge support from a David & Lucile Packard Fellowship and a Camille Dreyfus Teacher-Scholar award. BMS would like to thank a NASA Earth and Space Science Fellowship (NESSF NNX11AO06H), and JNH is grateful for support by a Robert & Carolyn Springborn fellowship and an NSF Graduate Research Fellowship (DGE 11-44245 FLLW). The authors would also like to thank Takeshi Oka for supplying the discharge cell and associated electronics and pumps used for this work.

References

(1) Wing, W.; Ruff, G.; Lamb, W.; Spezeski, J. *Phys. Rev. Lett.* **1976**, *36*, 1488–1491

(2) Gudeman, C. S.; Begemann, M. H.; Pfaff, J.; Saykally, R. J. *Phys. Rev. Lett.* **1983**, *50*, 727–731

(3) Stephenson, S. K.; Saykally, R. J. *J. Mol. Spectrosc.* **2005**, *231*, 145–153

(4) Gudeman, C. S.; Saykally, R. J. *Annu. Rev. Phys. Chem.* **1984**, *35*, 387–418

(5) Amano, T. *J. Chem. Phys.* **1983**, *79*, 3595

(6) Verbraak, H.; Ngai, A. K. Y.; Persijn, S. T.; Harren, F. J. M.; Linnartz, H. *Chem. Phys. Lett.* **2007**, *442*, 145–149

(7) Buhl, D.; Snyder, L. E. *Nat.* **1970**, *228*, 267–9

(8) Klemperer, W. *Nat.* **1970**, *227*, 1230–1230

(9) Woods, R.; Dixon, T.; Saykally, R.; Szanto, P. *Phys. Rev. Lett.* **1975**, *35*, 1269–1272

(10) Sanchez Contreras, C.; Sahai, R. *Astrophys. J.* **2004**, *602*, 960–977

(11) Purcell, C. R. et al. *Mon. Not. R. Astron. Soc.* **2006**, *367*, 553–576

(12) Liszt, H.; Lucas, R. *Astron. Astrophys.* **2004**, *428*, 445–450

(13) Milam, S. N.; Savage, C.; Ziurys, L. M.; Wyckoff, S. *Astrophys. J.* **2004**, *615*, 1054–1062

(14) Cazzoli, G.; Cludi, L.; Buffa, G.; Puzzarini, C. *Astrophys. J. Sup.* **2012**, *203*, 11

(15) Lattanzi, V.; Walters, A.; Drouin, B. J.; Pearson, J. C. *Astrophys. J.* **2007**, *662*, 771–778

(16) Crabtree, K. N.; Hodges, J. N.; Siller, B. M.; Perry, A. J.; Kelly, J. E.; II, P. A. J.; McCall, B. J. *Chem. Phys. Lett.* **2012**, *551*, 1 – 6

(17) Mills, A. A.; Siller, B. M.; McCall, B. J. *Chem. Phys. Lett.* **2010**, *501*, 1 – 5

(18) Donley, E. A.; Heavner, T. P.; Levi, F.; Tataw, M. O.; Jefferts, S. R. *Rev. Sci. Instrum.* **2005**, *76*, 063112

(19) Siller, B. M.; Porambo, M. W.; Mills, A. A.; McCall, B. J. *Opt. Express* **2011**, *19*, 24822–24827

(20) Hirota, E.; Endo, Y. *Journal of Molecular Spectroscopy* **1988**, *127*, 527 – 534

(21) Blake, G. A.; Laughlin, K. B.; Cohen, R. C.; Busarow, K. L.; Saykally, R. J. *Astrophys. J.* **1987**, *316*, L45–L48